Microscopic model of the timelike electromagnetic form factor of the nucleon

H. C. Dönges, M. Schäfer, and U. Mosel
Institut für Theoretische Physik, Universität Giessen, D-35392 Giessen, Germany
(Received 7 July 1994)

A microscopic model of the electromagnetic form factor of the nucleon is developed in a hadronic framework, including pions, nucleons, and the Δ resonance explicitly. The spacelike on-shell form factors are reproduced and predictions for the half off-shell dependence are made. The impact of this off-shell dependence in the timelike sector ($q^2 < 1$ GeV^2, thus including the region of vector meson dominance) is of main interest in this investigation.

PACS number(s): 13.40.Gp, 14.20.Dh

I. INTRODUCTION

Electromagnetic form factors of hadrons contain important information about the intrinsic structure of these particles and about their coupling to the external electromagnetic field. This electromagnetic structure has been explored mainly by electron scattering experiments, giving information on the electromagnetic form factor in the spacelike momentum region and thus on the spatial distribution of charges and magnetic moments inside the hadrons in general, and the nucleon in particular. The available data cover the momentum range from $q^2 = 0$ up to about $q^2 = 35$ GeV^2 and can be well parametrized by a dipole fit [1]. There exist models that explain the data by assuming a certain number of poles which all, unfortunately, are in the so-called "unphysical" region (not accessible by experiments on on-shell nucleons) [2,3].

The data are much more sparse for timelike momentum transfers, where the excitation of the nucleon and its decay are studied. Here the only available data come from experiments at LEAR, exploiting $p\bar{p}$ annihilation [4]. These data thus naturally start at momentum transfers larger than twice the mass of the proton. They show that conventional pole fits, e.g. [3], cannot be applied in this region any more. It is thus of special interest to explore the unphysical region and see whether there exists a rich structure of poles and thus whether the so-called vector meson dominance (VMD [5]), which underlies these pole fits, is a universal property of all hadrons or if it holds only for pions.

The region around momentum transfers corresponding to the vector meson mass (around 750–800 MeV for ρ and ω mesons) is so interesting because these pole fits predict here a very pronounced resonance structure in the form factors [3]. Since access to this region for on-shell protons is impossible, the only alternative is to look for half off-shell processes. Indeed, dilepton production in hadronic collisions (bremsstrahlung dileptons) offers access to the half off-shell electromagnetic form factor in the timelike region [6].

Experiments of this kind have been performed by the DLS Collaboration for $p+p$, $p+A$, and $A+A$ collisions [7]. Simulations of these processes show for $p + p$ and $p + A$ a clear window for these bremsstrahlung contributions where these are not overshadowed by other processes [8]; for $A + A$ a strong ω peak is predicted [9].

Under the assumption of VMD the elementary dilepton production processes $NN \to NNe^+e^-$, $\pi N \to Ne^+e^-$, and $\gamma N \to Ne^+e^-$ were studied by the Giessen group [6,10,11]. It is, however, unclear if the timelike electromagnetic form factor is influenced by the off-shellness of the intermediate nucleon. The purpose of this paper is to model the relevant vertex, to study its off-shell dependence, and to investigate if VMD is still visible if this off-shell dependence is properly taken into account. The calculations are thus meant to stimulate and to provide some guidance for experimental investigations of this important hadronic property.

To obtain the general vertex, one needs a dynamical model that describes the electromagnetic structure of the nucleon. It would be most desirable to use the quark degrees of freedom. Unfortunately, state of the art quark models of the nucleon do not allow one to study off-shell effects and excitations quantitatively, but only in a qualitative way. Their success is mainly confined to spacelike properties of real nucleons at the present time [12]. In this paper, therefore, all calculations are performed using hadronic degrees of freedom, following the concept of Naus and Koch [13] or Tiemeijer and Tjon [14], who performed similar calculations for the spacelike regime.

From a spectral analysis of form factors [15] one has learned about two important ingredients: πN scattering and $\pi\pi$ scattering. While $\pi\pi$ scattering is resonant, and thus in this channel best described by taking into account a coupling to the ρ meson, πN scattering is more difficult to implement, and will be handled only in a very schematic way in the present model. On the other hand, semiphenomenological models [16,17] show the success of a description of the form factors in a cloud/core picture. This will be discussed later in this paper.

Constrained by gauge invariance of the electromagnetic interaction, the vertex is constructed from a pion loop expansion of the nucleon propagator by coupling external photons to each charged particle in the loop. In this loop expansion the Δ resonance is taken into account because, first of all, it is necessary for the reproduction of πN scattering, and secondly it is the first important resonance to contribute to the off-shell effects. In addition to that,

from an analysis of the Gerasimov-Drell-Hearn sum rule [18], the Δ is found to be most important to understand the anomalous magnetic moments of the nucleons.

This paper is organized as follows. In Sec. II, the general structure of form factors for nucleons and pions is discussed, and gauge invariance and its consequences are introduced. In Sec. III, the model is presented, and gauge invariance is proven for a simple case. A discussion of VMD in this context is given in Sec. IV. Results and comparison to data are shown in Sec. V. Section VI concludes the paper.

II. GENERAL STRUCTURE OF FORM FACTORS

A. Form factor of nucleons

The most general form of the electromagnetic interaction vertex for nucleons can be split into an isoscalar part and an isovector part:

$$\Gamma^\mu(p',p) = \Gamma^\mu_S(p',p) + \tau_3\Gamma^\mu_V(p',p) \quad . \tag{1}$$

The vertices of proton or neutron are then linear combinations $\Gamma^\mu_p(p',p) = \Gamma^\mu_S(p',p) + \Gamma^\mu_V(p',p)$, $\Gamma^\mu_n(p',p) = \Gamma^\mu_S(p',p) - \Gamma^\mu_V(p',p)$.

The isoscalar or isovector parts can be split up further. Let p denote the four-momentum of the incoming nucleon, p' the four-momentum of the outgoing nucleon, and $q = p - p'$ the four-momentum of the outgoing photon. This choice is more convenient for the case of timelike momentum transfer and for dilepton production, but is different from what is conventionally used in the literature, where q is the four-momentum of the incoming photon; this amounts to some sign changes in the decomposition of the vertex compared to other papers [13,14,19]. According to [19] the isoscalar/isovector vertex can be expressed as

$$\Gamma^\mu_{S,V}(p',p) = e\sum_{r',r=0}^{1}\{\gamma\cdot p'\}^{r'}\left(A^{r'r}_{1S,V}\gamma^\mu - A^{r'r}_{2S,V}\frac{i\sigma^{\mu\nu}q_\nu}{2m} - A^{r'r}_{3S,V}q^\mu\right)\{\gamma\cdot p\}^r \quad . \tag{2}$$

The 24 functions $A^{r'r}_{iS,V}$ ($i = 1,\ldots,3; r,r' = 0,1$) are scalar functions of the three variables p^2, p'^2, and q^2. Introducing a shorthand notation

$$\mathcal{O}^\mu_1 = \gamma^\mu, \quad \mathcal{O}^\mu_2 = -\frac{i\sigma^{\mu\nu}q_\nu}{2m}, \quad \mathcal{O}^\mu_3 = -q^\mu,$$

(m = nucleon mass)

and the projection operator

$$\Lambda^s(p) = \frac{s\gamma\cdot p + W}{2W} \quad \text{with } W = \sqrt{p^2}, \quad s = \pm 1 \quad , \tag{3}$$

(2) can be written as (dropping S and V for convenience)

$$\Gamma^\mu(p',p) = e\sum_{i=1}^{3}\sum_{s,s'=\pm1}\Lambda^{s'}(p')F_i^{s's}(W',W;q^2)\mathcal{O}^\mu_i\Lambda^s(p). \tag{4}$$

The functions $F_i^{s's}$ are linear combinations of the $A_i^{r'r}$.

Since for $p^2 = m^2$ the operator $\Lambda^s(p)$ is just the projection operator to positive ($s = +1$) or negative ($s = -1$) energies, $\Gamma^\mu(p',p)$ taken between on-shell spinors reduces to

$$\bar u(p')\Gamma^\mu(p',p)u(p) = e\sum_{i=1}^{3}\bar u(p')F_i^{++}(m,m;q^2)\mathcal{O}^\mu_i u(p) \quad .$$

It turns out that $F_3^{++}(m,m;q^2) = 0$ (time reversal invariance), so the on-shell vertex takes on the well known form [20]

$$\bar u(p')\Gamma^\mu(p',p)u(p) = e\bar u(p')\left[F_1^{++}(q^2)\gamma^\mu - F_2^{++}(q^2)\frac{i\sigma^{\mu\nu}q_\nu}{2m}\right]u(p) \quad .$$

At $q^2 = 0$ the form factor F_1^{++} measures the electric charge and F_2^{++} measures the anomalous magnetic moment.

The vertex $\Gamma^\mu(p',p)$ contains self energy corrections in the external legs. For this reason it is often called a *reducible* vertex. In this paper it is also called a *full* vertex in order to indicate that in experimental measurements these self energy corrections are always included. To eliminate these corrections, the *irreducible* vertex is defined by

$$S(p')\Gamma^\mu_{\rm irr}(p',p)S(p) = S_0(p')\Gamma^\mu(p',p)S_0(p) \quad . \tag{5}$$

For the irreducible vertex a decomposition exists similar to the one for the full vertex, as will be proven now. In (5) $S_0(p)$ is the free propagator, and $S(p)$ is the full propagator, including all self energy corrections $\Sigma(p) = S_0^{-1}(p) - S^{-1}(p)$. Most generally $\Sigma(p)$ is decomposed into a vector part $\Sigma_V(W)$ and a scalar part $\Sigma_S(W)$ by $\Sigma(p) = \Sigma_V(W)\gamma\cdot p - \Sigma_S(W)m$, so the full propagator takes on the form

$$\begin{aligned} S^{-1}(p) &= \gamma\cdot p - m - \Sigma(p) \\ &= \gamma\cdot p[1-\Sigma_V(W)] - m[1-\Sigma_S(W)] \\ &= \gamma\cdot p^* - m^* \, . \end{aligned}$$

It proves helpful to introduce the positive and negative energy projections of the self energy and the propagator $\Sigma^\pm(W)$ and $S^\pm(W)$ by

$$\Sigma(p) = \sum_{s=\pm1}\Lambda^s(p)\Sigma^s(W), \quad S(p) = \sum_{s=\pm1}\Lambda^s(p)S^s(W) \quad .$$

Using the properties of the projection operators

$$\Lambda^+(p) + \Lambda^-(p) = 1, \quad \Lambda^+(p) - \Lambda^-(p) = \frac{\gamma\cdot p}{W} \quad , \tag{6}$$

one finds for the self energy

$$\Sigma^s(W) = s\Sigma_V(W)W - \Sigma_S(W)m \tag{7}$$

and for the full propagator

$$S^s(W) = \frac{1}{sW^* - m^*} = \frac{1}{sW - m - \Sigma^s(W)} \quad , \tag{8}$$

where $W^* = W[1 - \Sigma_V(W)]$ and $m^* = m[1 - \Sigma_S(W)]$. With this notation one finds further

$$S_0(p) = \sum_s \Lambda^s(p) S_0^s(W), \quad S_0^s(W) = \frac{1}{sW - m} \ , \tag{9}$$

$$S^{-1}(p) = \sum_s \Lambda^s(p) S^{-1^s}(W), \quad S^{-1^s}(W) = sW^* - m^* \ , \tag{10}$$

$$S_0^{-1}(p) = \sum_s \Lambda^s(p) S_0^{-1^s}(W), \quad S_0^{-1^s}(W) = sW - m \ . \tag{11}$$

Now one can easily derive the relation between the reducible vertex (4) and the irreducible vertex (5):

$$\begin{aligned}\Gamma^\mu_{\rm irr}(p',p) &= S^{-1}(p')S_0(p')\Gamma^\mu(p',p)S_0(p)S^{-1}(p) \\ &= e\sum_{i=1}^{3}\sum_{s's} \Lambda^{s'}(p')\frac{s'W'^* - m'^*}{s'W' - m} F_i^{s's}(W',W;q^2)\frac{sW^* - m^*}{sW - m}\mathcal{O}_i^\mu \Lambda^s(p) \\ &= e\sum_{i=1}^{3}\sum_{s's} \Lambda^{s'}(p') f_i^{s's}(W',W;q^2)\mathcal{O}_i^\mu \Lambda^s(p) \quad .\end{aligned} \tag{12}$$

Equation (12) represents the desired decomposition of the irreducible vertex in terms of the irreducible form factors $f_i^{s's}(W',W;q^2)$.

The Ward-Takahashi identity (WTI) relates the irreducible vertex to the full propagator [21]:

$$q_\mu \Gamma^\mu_{\rm irr}(p',p) = e\hat{Q}[S^{-1}(p) - S^{-1}(p')] \quad . \tag{13}$$

$\hat{Q}$ is the appropriate charge operator.

Two useful identities will be introduced here:

$$\Lambda^{s'}(p')\gamma \cdot q \Lambda^s(p) = \Lambda^{s'}(p')(sW - s'W')\Lambda^s(p) \ , \tag{14}$$

$$\begin{aligned}-\Lambda^{s'}(p')i\sigma_{\mu\nu}q^\nu\Lambda^s(p) = \Lambda^{s'}(p')[&(sW + s'W')\gamma_\mu \\ &-(p+p')_\mu]\Lambda^s(p) \quad .\end{aligned} \tag{15}$$

(15) is a general form of the Gordon identity [20]. With the use of (14) and $q_\mu \mathcal{O}_2^\mu = 0$ the projection of (13) onto positive and negative states yields

$$\begin{aligned}&f_1^{s's}(sW - s'W') - q^2 f_3^{s's} \\ &\quad = \hat{Q}[S^{-1^s}(W) - S^{-1^{s'}}(W')] \\ &\quad = \hat{Q}[(sW^* - s'W'^*) - (m^* - m'^*)] \quad .\end{aligned} \tag{16}$$

For the case of an outgoing on-shell particle ($W' = m$) of positive energy ($s' = +1$) this reduces to

$$f_1^{+s} - \frac{q^2}{sW - m} f_3^{+s} = \hat{Q}\frac{sW^* - m^*}{sW - m} \tag{17}$$

or for the full form factor [(17) $\times \frac{sW - m}{sW^* - m^*}$]:

$$F_1^{+s} - \frac{q^2}{sW^* - m^*} F_3^{+s} = \hat{Q} \quad . \tag{18}$$

To get (18) one needs further $\left.\frac{W' - m}{W'^* - m'^*}\right|_{W' = m} = 1$, i.e., the full propagator has a pole of unit residue at the physical mass m of the nucleon.

For real photons ($q^2 = 0$) one recovers that $F_1^{+s} = 1$ for protons and $F_1^{+s} = 0$ for neutrons. This holds for the full form factor even if the incoming nucleon is off shell. Note that (17) implies that $f_1^{+s}(q^2 = 0)$ depends on the nucleon's off-shellness and only reduces to the real charge for on-shell incoming particles. The latter must be true because for on-shell particles there is no difference between the full and the irreducible vertex.

Note that the WTI does not pose any constraint on the magnetic form factors F_2^{+s}. Note also that $F_3^{+s}(m,m;q^2) = f_3^{+s}(m,m;q^2)$ have to vanish for all q^2 in order to obtain finite contributions on the left-hand side of (17) and (18).

To obtain the full vertex, the knowledge of the full propagator is needed, which can be obtained from f_1^{+s} using relation (17) taken at $q^2 = 0$:

$$S^{-1s}(W) = sW^* - m^* = f_{1,p}^{+s}(m,W;q^2 = 0)(sW - m) \quad .$$

The index p stands for proton. This allows one to write the half off-shell full form factor as

$$F_i^{+s}(m,W;q^2) = \frac{f_i^{+s}(m,W;q^2)}{f_{1,p}^{+s}(m,W;0)} \quad . \tag{19}$$

It is thus sufficient to calculate the irreducible vertex only.

From (16) more relations can be derived especially for $q^2 = 0$:

$$\begin{aligned}&f_1^{++}(W,m;0) = f_1^{++}(m,W;0) \ , \\ &f_1^{+-}(m,W;0) = f_1^{-+}(W,m;0) \ , \\ &f_{1,p}^{--}(m,m;0) = 1, \quad f_{1,n}^{--}(m,m;0) = 0 \quad .\end{aligned}$$

So the off-shell full form factor is

$$F_i^{s's}(W',W;q^2) = \frac{f_i^{s's}(W',W;q^2)}{f_{1,p}^{s'+}(W',m;0)f_{1,p}^{+s}(m,W;0)} \quad . \tag{20}$$

Experiments always measure the full form factor. $F_3^{s's}$ is never accessible by experiments since $\mathcal{O}_3^\mu j_\mu = 0$ for any conserved current j_μ.

B. Form factor of pions

The most general form of the pion-photon vertex is [22]

$$\Gamma_\pi^\mu(p',p) = e\hat{Q}_\pi[f_1(p'^2,p^2;q^2)p'^\mu + f_2(p'^2,p^2;q^2)p^\mu] \quad .$$

A more convenient and also better known notation is

$$\Gamma_\pi^\mu(p',p) = e\hat{Q}_\pi[A(p'^2,p^2;q^2)P_L^\mu + B(p'^2,p^2;q^2)P_T^\mu]$$

with $P_L = p' + p$, $P_T = P_L - q(P_L \cdot q/q^2)$, and $q = p - p'$.

If j_μ is a conserved current, one measures

$$j_\mu\Gamma_\pi^\mu(p',p) = e\hat{Q}_\pi[A(p'^2,p^2;q^2) + B(p'^2,p^2;q^2)]j_\mu P_L^\mu \quad ,$$

i.e., the sum of A and B. The WTI requires

$$\begin{aligned} q_\mu\Gamma_\pi^\mu(p',p) &= e\hat{Q}_\pi q_\mu P_L^\mu A(p'^2,p^2;q^2) \\ &= e\hat{Q}_\pi[D_\pi^{-1}(p^2) - D_\pi^{-1}(p'^2)] \quad . \end{aligned}$$

Thus only A is constrained by the WTI.

The on-shell form factor of pions is a measurable quantity. It is given to good precision by the vector meson dominance (VMD) hypothesis [23]. In fact, the VMD hypothesis works so well that one is led to assume that the bare pion is essentially a structureless particle [24]. It is therefore safe to neglect effects of the pion's off-shellness and to assume that A and B depend on q^2 only:

$$j_\mu\Gamma_\pi^\mu(p',p) = e\hat{Q}_\pi F_\pi(q^2)j_\mu P_L^\mu \quad ,$$

where $F_\pi(q^2)$ is the measured form factor. This fixes $B(q^2)$:

$$B(q^2) = F_\pi(q^2) - A(q^2) \quad .$$

Given any form of the pion self energy, this allows one to maintain gauge invariance as well as the measured form factor. Section IV will explain the VMD hypothesis and will show how to carry it over to the nucleon.

III. MODEL FOR THE FORM FACTOR

As mentioned in the Introduction, there exists a subtle interplay of πN and $\pi\pi$ scattering in describing the electromagnetic properties of nucleons. This section is devoted to introducing the part of the model that is suited to describe the πN interaction. Subsection III A introduces the Lagrangians for nucleons, pions, and Δ's. In a naive picture the coupling of photons is introduced. Subsection III B describes the coupling of the photon to these fields in the correct way and shows that this is equivalent to the picture developed in subsection III A, which thus respects the local U(1) symmetry of QED. In Sec. IV the $\pi\pi$ interaction is modeled in terms of vector meson dominance.

A. Interaction of mesons, baryons, and photons

Part of the structure of the nucleon is due to the meson cloud that dresses the bare nucleon. This idea is well established and several phenomenological models exist that take it into account [16,17]. For electromagnetic form factors Naus and Koch [13], Tiemeijer and Tjon [14] or Bos *et al.* [25] performed detailed calculations based on a meson-baryon interaction picture, all giving essentially the same results for the shape and the off-shell dependence of the form factors, but differing somewhat in their predictions for the anomalous magnetic moments. However, these authors restricted themselves to spacelike momentum transfer and to off-shell nucleons with $W < m + m_\pi$ in order to avoid poles due to decay into inelastic channels. Since the purpose of this paper is to compute the form factor in the timelike region, the decay modes have to be included; also, the Δ resonance will be considered in the calculation because for off-shell nucleons with $W > m$ the Δ is no longer kinematically suppressed.

The model used here is based on the Lagrangian densitiy for pions and nucleons with pseudovector coupling.

$$\begin{aligned} \mathcal{L}_N = \bar{\Psi}(\gamma\cdot p - m)\Psi + \frac{1}{2}[(\partial_\mu\tilde{\pi})^\dagger(\partial^\mu\tilde{\pi}) - m_\pi^2\tilde{\pi}^\dagger\tilde{\pi}] \\ + \frac{g_{NN\pi}}{2m}\bar{\Psi}\gamma_5\gamma^\mu\tilde{\tau}\Psi\partial_\mu\tilde{\pi} \quad . \end{aligned} \tag{21}$$

Including the Δ leads to an additional term in (21):

$$\mathcal{L}_\Delta = \bar{\Psi}_\Delta^\mu\Lambda_{\mu\nu}\Psi_\Delta^\nu + \frac{g_{N\Delta\pi}}{2m}\left(\bar{\Psi}_\Delta^\mu\tilde{T}\Psi\partial_\mu\tilde{\pi} + \text{H.c.}\right) \tag{22}$$

with

$$\begin{aligned} \Lambda_{\mu\nu} = (\gamma\cdot p - m_\Delta)g_{\mu\nu} - (\gamma_\mu p_\nu + p_\mu\gamma_\nu) + \gamma_\mu\gamma\cdot p\gamma_\nu \\ + m_\Delta\gamma_\mu\gamma_\nu \quad , \end{aligned} \tag{23}$$

as derived in the Rarita-Schwinger formalism [26,27]; $\tilde{T}$ is the matrix that couples isospin 3/2 to isospin $1/2 \oplus 1$. The Δ is here treated as a stable particle; its finite decay width must be neglected at the order of diagrams discussed here. Using a momentum dependent width would amount to including self energy corrections to the Δ propagator; this corresponds to diagrams of higher order in pion lines. Also, a whole set of new diagrams would be necessary to maintain gauge invariance. On the other hand, a constant width in the Δ propagator always yields complex form factors, even for on-shell nucleons, because the relevant thresholds are not taken into account.

This subsection will describe how the corrections to the electromagnetic interaction vertex can be constructed for diagrams including one pion loop. The starting point will be the nucleon propagator, which is up to the one-pion-loop level given by Fig. 1. In the naive picture the photon couples to all charged particles individually. That this indeed fulfills the WTI will be proven in the following subsection. The irreducible vertex is given by Fig.

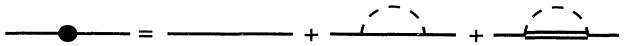

FIG. 1. Expansion of the full nucleon propagator in first order in pion lines. The nucleon propagator is displayed by the solid single line, the Δ propagator by the solid double line, the full propagator by the solid line with the fat dot, and the pion propagator by the dashed line.

2, where the coupling of the photon to the hadrons is according to the usual Feynman rules. Since the pion coupling is chosen to be pseudovector, additional contact terms arise [Figs. 2(d) and 2(e)].

Since all the loop diagrams diverge, a regularization by a covariant cutoff of the form

$$f_c(q^2) = \frac{m_\pi^2 - \Lambda^2}{q^2 - \Lambda^2} = (m_\pi^2 - \Lambda^2) D_c(q) \qquad (24)$$

is used. This form of the cutoff is chosen because it can be visualized as the propagator $D_c(q)$ of a particle of mass Λ with the same quantum numbers as the pion; this fictitious cutoff particle will be called the COP. The $NN\pi$ vertex is regulated with the monopole form, whereas the $N\Delta\pi$ vertex needs a dipole cutoff to yield convergence because the Δ propagator is $\mathcal{O}(p)$. In the spirit of the previous paragraph the photon will then also couple to the COP if the intermediate pion carries charge. The photon-pion coupling must therefore be replaced by a sum of vertices given in Fig. 3; the double dashed line denotes the propagator of the COP. The diagrams with an internal Δ propagator have two COP propagators because of the dipole cutoff. The pion-photon vertex in this case must thus be replaced by five diagrams.

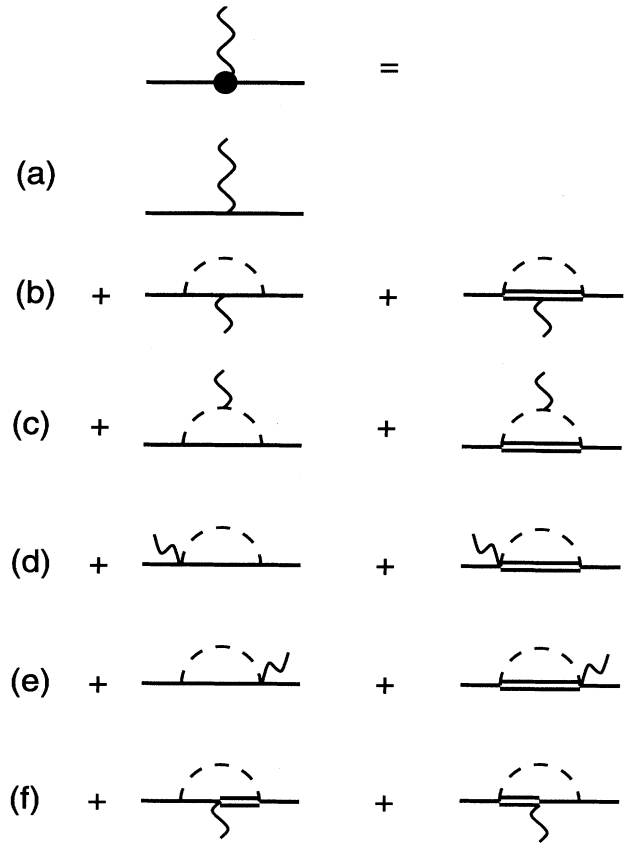

FIG. 2. Loopwise expansion of the irreducible nucleon vertex. (a) is the free vertex, (b) and (c) come from coupling of photons to charged hadron lines of the propagator in Fig. 1, (d) and (e) arise from contact terms due to pseudovector coupling of pions to nucleon and Δ, and (f) is the contribution of the decay $\Delta \to N\gamma$.

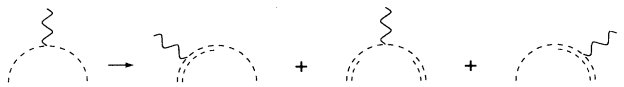

FIG. 3. Additional diagrams to satisfy the WTI if a cutoff is introduced in the πN or the $\pi\Delta$ vertex. The double dashed line represents the propagator of the COP.

The mass of the COP must be chosen large enough so that unphysical decay modes are avoided. The possible decay modes and thus contributions to the imaginary part of the form factor can be found by applying the usual cutting rules. If the incoming nucleon is far enough off shell ($W > m + m_\pi$) it can decay into an on-shell nucleon and a real pion as depicted in Fig. 4(a). In principle the off-shell nucleon can also decay into a nucleon and a COP if $W > m + \Lambda$. This inequality sets the limit of the model. For the case of this paper $W_{\max}$ will be restricted to 2 GeV, so Λ should be somewhat larger than 1 GeV. This is in good agreement with cutoff values used in meson exchange potentials. If the cut is taken as indicated in Fig. 4(b) it becomes clear that there is also a restriction on the invariant mass M of the photon. If $M = \sqrt{q_\gamma^2} > 2m_\pi$, $\pi^+\pi^-$ production becomes possible. Pion-COP production is not possible if M is restricted to $M < m_\pi + \Lambda \approx m_\pi + W_{\max} - m \approx 1$ GeV.

B. Ward-Takahashi identity

This subsection is devoted to the proof of correctness of the picture developed above. First, the appropriate electromagnetic interaction vertex will be derived from the Lagrangians (21) and (22) by minimal coupling. Then the "reduced" formalism will be introduced to keep track of the COP. Finally it will be proven that the WTI is fulfilled.

Since the photon is the gauge field of local U(1) symmetry, it is introduced into the Lagrangian by substituting $p_\mu \to p_\mu - e\hat{Q}A_\mu$, where $\hat{Q}$ is the charge operator. This leads to the usual interaction terms for nucleons and pions:

$$\mathcal{L}_{\rm em}^N = -e\bar{\Psi}\gamma^\mu \hat{Q}_N \Psi A_\mu - ie\tilde{\pi}^\dagger \left(\frac{\overrightarrow{\partial}}{\partial x_\mu} - \frac{\overleftarrow{\partial}}{\partial x_\mu} \right) \hat{Q}_\pi \tilde{\pi} A_\mu \quad ,$$

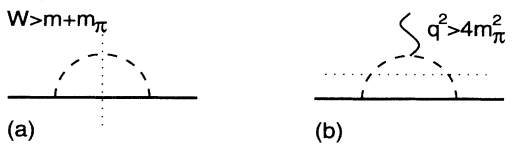

FIG. 4. Possible cuts of the loop diagrams. The cut in (a) corresponds to the decay of the off-shell internal nucleon to an on-shell nucleon and a pion; the cut in (b) corresponds to $\pi^+\pi^-$ annihilation if the photon has high enough invariant mass, or to two-pion production if the incoming nucleon is far enough off shell.

to a contact term because of the derivative in the pseudovector coupling of pions and nucleons:

$$\mathcal{L}^c_{\rm em} = -e\frac{g_{NN\pi}}{2m}\bar{\Psi}\gamma_5\gamma^\mu\tilde{\tau}\Psi\hat{Q}_\pi\tilde{\pi}A_\mu \quad ,$$

and to terms from $\mathcal{L}_\Delta$:

$$\begin{aligned}\mathcal{L}^\Delta_{\rm em} = &-e\bar{\Psi}^\mu_\Delta(\gamma_\lambda g_{\mu\nu}+\gamma_\mu g_{\lambda\nu}+\gamma_\nu g_{\lambda\mu}\\ &-\gamma_\mu\gamma_\lambda\gamma_\nu)\hat{Q}_\Delta\Psi^\nu_\Delta A^\lambda\\ &-e\frac{g_{N\Delta\pi}}{2m}\left(\bar{\Psi}^\mu_\Delta\tilde{T}\Psi\hat{Q}_\pi\tilde{\pi}A_\mu+\text{H.c.}\right) \quad .\end{aligned}$$

The operators $\hat{Q}_{\pi,N,\Delta}$ return the appropriate charge. Since the Δ can decay into a γ and a nucleon, an additional term must be included in the Lagrangian:

$$\mathcal{L}_{\Delta\to n\gamma} = i\frac{g_{\Delta N\gamma}}{2m}(\bar{\Psi}^\mu_\Delta\gamma_5\gamma^\nu T^3\Psi F_{\mu\nu}+\text{H.c.}) \quad .$$

The corresponding vertex is $\gamma_5(\gamma^\nu q^\mu-\gamma\cdot q g^{\mu\nu})G_1$ where the factor $\sqrt{2/3}$ from T^3 and the coupling constant have been absorbed in G_1. According to [28] this vertex is mainly responsible for the $M1$ multipole which dominates the decay. q is the momentum of the outgoing photon. Note that the index μ of the above vertex contracts with the Δ, while the index ν contracts with the photon field.

To prove gauge invariance of the model developed in this paper, three steps need to be done. To obtain a gauge invariant coupling to the pion, the coupling to the COP needs to be investigated, as well. So, first, the COP-photon interaction vertex is constructed, and then, as a second step, the effective pion-photon vertex is constructed to fulfill the WTI locally using the reduced formalism of Gross and Riska [22]. The third step is to actually prove the WTI for the photon-nucleon interaction.

Since the COP is not a fundamental particle, it does not appear in the Lagrangian. Therefore so far it does not interact with the electromagnetic field. To obtain gauge invariance it needs the same interaction vertex as the pion:

$$\Gamma^\mu_{cc\gamma}(p',p) = \Gamma^\mu_{\pi\pi\gamma}(p',p) = e\hat{Q}_\pi(p+p')^\mu \quad ,$$

where p and p' are the momenta of the incoming and outgoing particles, respectively. Note that the vertex so constructed obviously fulfills the WTI of a free particle:

$$\begin{aligned}(p-p')_\mu\Gamma^\mu_{cc\gamma}(p',p) &= e\hat{Q}_\pi(p^2-p'^2)\\ &= e\hat{Q}_\pi\left[D_c^{-1}(p)-D_c^{-1}(p')\right] \quad . \quad (25)\end{aligned}$$

Next the reduced formalism is introduced. This part of the paper follows closely [22], whose authors treat the cutoff function f_c as a contribution to the pion polarization function, which is possible because f_c is a function of the pion momentum only. The reduced pion propagator $D_R(p)$ is defined as

$$D_R(p) = f_c(p^2)D_\pi(p)f_c(p^2) \equiv \frac{1}{p^2-m_\pi^2-\Pi(p^2)} \quad ,$$

which defines the polarization function to be

$$\Pi(p^2) = (p^2-m_\pi^2)[1-f_c^{-2}(p^2)] \quad .$$

It has the necessary properties $\Pi(p^2=m_\pi^2)=0$, $\partial\Pi/\partial p^2|_{p^2=m_\pi^2} = 1-f_c^{-2}(m_\pi^2)=0$ because $f_c(m_\pi^2)=1$. Thus $D_R(p)$ can be viewed as the *full* propagator in this model.

The WTI requires a relation between the *full* propagator and the *irreducible* vertex:

$$(p-p')_\mu\Gamma^\mu_{\rm irr}(p',p) = e\hat{Q}_\pi\left[D_R^{-1}(p)-D_R^{-1}(p')\right] \quad .$$

Multiplying by the full propagator on each side gives the requirement

$$\begin{aligned}&(p-p')_\mu D_R(p')\Gamma^\mu_{\rm irr}(p',p)D_R(p)\\ &\qquad = e\hat{Q}_\pi\left[D_R(p')-D_R(p)\right] \quad . \quad (26)\end{aligned}$$

Requirement (26) can be satisfied with the following choice for the irreducible vertex:

$$\begin{aligned}\Gamma^\mu_{\rm irr}(p',p) = (m_\pi^2-\Lambda^2)^2[&\Gamma^\mu_{cc\gamma}(p',p)D_c(p)D_\pi(p)\\ &+D_\pi(p')\Gamma^\mu_{\pi\pi\gamma}(p',p)D_\pi(p)\\ &+D_\pi(p')D_c(p')\Gamma^\mu_{cc\gamma}(p',p)] \quad ,\end{aligned}$$

where $\Gamma^\mu_{cc\gamma}(p',p)$ and $\Gamma^\mu_{\pi\pi\gamma}(p',p)$ are the individual vertices of the free particles. This is pictorially represented in Fig. 3 and can be shown as follows:

$$\begin{aligned}(p-p')_\mu D_R(p')\Gamma^\mu_{\rm irr}(p',p)D_R(p) &= (m_\pi^2-\Lambda^2)^2e\hat{Q}_\pi\{D_c(p')[D_c^{-1}(p)-D_c^{-1}(p')]D_c(p)D_\pi(p)D_c(p)\\ &\quad +D_c(p')D_\pi(p')[D_\pi^{-1}(p)-D_\pi^{-1}(p')]D_\pi(p)D_c(p)\\ &\quad +D_c(p')D_\pi(p')D_c(p')[D_c^{-1}(p)-D_c^{-1}(p')]D_c(p)\}\\ &= (m_\pi^2-\Lambda^2)^2e\hat{Q}_\pi\left[D_c(p')D_\pi(p')D_c(p')-D_c(p)D_\pi(p)D_c(p)\right]\\ &= e\hat{Q}_\pi[D_R(p')-D_R(p)] \quad ,\end{aligned}$$

using the definition of $D_c(p)$ in (24) and the fact that the free vertex fulfills the WTI with the free propagator (25).

The naive picture, developed in the previous subsection, to couple a photon to each of the charged particles then very naturally emerges from the requirement of gauge invariance. This simplifies the numerical treatment of such processes considerably because the self energy of the pion need not be constructed explicitly; only free propagators occur, and, therefore, the pole structure is much more transparent.

On the other hand, the reduced formalism provides a simple way to prove gauge invariance of the model.

This is demonstrated for the exemplary case of a nucleon-pion loop, where, in order to reduce the effort, the pseudoscalar coupling is used. The results also hold for the pseudovector case if the contact terms are taken into account. For the proof only two diagrams need to be considered: the photon couples to the internal nucleon [Fig. 2(b)], and the photon couples to the internal pion [Fig. 2(c)]. The pion propagator must be replaced by the reduced propagator and the vertex correspondingly by the irreducible vertex. For the moment the isospin factors are neglected; at the end they will be considered for protons and neutrons separately. With $q_\mu = (p - p')_\mu$ one gets for diagram 2(c) using (26)

$$q_\mu \int \frac{d^4k}{(2\pi)^4} g\gamma_5 iS_0(k) g\gamma_5 iD_R(p'-k)(-i)\Gamma^\mu_{\rm irr}(p'-k, p-k) iD_R(p-k)$$

$$= e \int \frac{d^4k}{(2\pi)^4} g\gamma_5 iS_0(k) g\gamma_5 i\hat{Q}_\pi [D_R(p'-k) - D_R(p-k)] \quad . \quad (27)$$

Equation (27) is equal to the difference of self energy diagrams, but, since $\hat{Q}_\pi$ is still left in the expression, it is only that part of the self energy which is due to charged pions. The remaining contribution of the neutral pion comes from diagram 2(b):

$$q_\mu \int \frac{d^4k}{(2\pi)^4} g\gamma_5 iS_0(p'-k)(-ie\hat{Q}_N\gamma^\mu) iS_0(p-k) g\gamma_5 iD_R(k)$$

$$= -e \int \frac{d^4k}{(2\pi)^4} g\gamma_5 S_0(p'-k)\hat{Q}_N [S_0^{-1}(p-k) - S_0^{-1}(p'-k)] S_0(p-k) g\gamma_5 D_R(k)$$

$$= e \int \frac{d^4k}{(2\pi)^4} g\gamma_5 i\hat{Q}_N [S_0(p'-k) - S_0(p-k)] g\gamma_5 iD_R(k) \quad . \quad (28)$$

For an incoming proton only the $\pi^+ n$ loop contributes to (27) and gives an isospin factor 2; the $\pi^0 p$ loop contibutes to (28) with an isospin factor 1. Adding both, one finds exactly $e[\Sigma(p') - \Sigma(p)]$. For an incoming neutron the $\pi^- p$ loop contributes to both diagrams with a factor of 2; however, since the charge operators are present, there is a relative minus sign between (27) and (28), such that they cancel exactly. The $\pi^0 n$ loop contributes to neither diagram.

The WTI requires for the nucleon

$$q_\mu \Gamma^\mu_{NN\gamma}(p', p)$$

$$= e\hat{Q}_N [S^{-1}(p) - S^{-1}(p')]$$
$$= e\hat{Q}_N [\gamma \cdot p - m - \Sigma(p) - \gamma \cdot p' + m + \Sigma(p')]$$
$$= e\hat{Q}_N [\gamma \cdot q + \Sigma(p') - \Sigma(p)] \quad .$$

Obviously the direct term [Fig. 2(a)] accounts for the $\gamma \cdot q$ whereas the vertex corrections exactly make up for the self energy. This proves gauge invariance up to the desired order in the strong coupling constant. The proof for pseudovector coupling or for the case of an internal Δ follows the same scheme as outlined above.

With the presented method the electromagnetic vertex correction can be constructed from the self energy given to the desired order in the strong coupling constant. It is given by just adding external photon lines to each propagator corresponding to a charged particle. If a cutoff function is needed it can be absorbed in the reduced formalism, which is powerful enough to allow a proof of gauge invariance, on one hand, and simple to implement numerically, on the other hand.

IV. ROLE OF VECTOR MESON DOMINANCE

The idea of vector meson dominance was first introduced by Sakurai [5]. It supposes that the photon couples to the hadron by first converting to a vector meson (a ρ meson specifically), which then couples to the hadron. The idea was first investigated for the electromagnetic form factor of the pion, where it turned out to be successful. For timelike momentum transfers the structure of the ρ-meson propagator shows up clearly. Furthermore, based on the assumption that the ρ meson is the "gauge boson" of local isospin rotation, Sakurai introduced the vector meson universality hypothesis, which states that the ρ meson couples to all hadrons with the same universal coupling constant g_ρ, which is equal to the ρ-γ coupling constant $g_{\rho\gamma}$. If this is true, the electromagnetic form factor of the proton should have the same shape as that of the pion.

From electron scattering on nucleons one knows that the spacelike form factors are well described by the dipole fit [1]. This is not in agreement with the simple assumption of VMD, which always results in monopole form factors. For this reason a number of resonances besides the ρ meson are introduced. Their coupling constants to the nucleon are determined by a fit to the data [2,3], in a so-called pole fit. In the calculations of Ref. [2], furthermore, information on πN scattering is included. By constrain-

ing the coupling constants it is possible to eliminate the leading monopole term and thus to obtain a dipole shape.

These pole fits can be analytically continued into the unphysical region (nucleon on mass shell, timelike momentum transfer of the photon below the $N\bar{N}$ threshold). A rich, dominant pole structure shows up, which — if it were observable — would contribute a direct proof of VMD for the nucleon. The pole fits also predict the behavior of the form factors in the timelike region above the $N\bar{N}$ threshold. Recent data taken at LEAR [4] show disagreement with the fit obtained by [3] on the basis of the VMD hypothesis.

It was pointed out by Höhler and Pietarinen [15] that, besides the poles in $\pi^+\pi^-$ annihilation, the process $N\bar{N} \to \pi^+\pi^-$ is also important to describe the form factor of the nucleon. The failure of the pole fit of [3] most probably is linked to this. It is thus an interesting question to investigate if πN scattering influences the picture of VMD considerably.

Since the information is hidden in the unphysical region, the experiments must be performed using off-shell nucleons. It must thus be checked if the off-shell dependence of the form factor interferes with the VMD picture. In this section a scheme is set up to model VMD for pions as well as for nucleons, which in Sec. V will be combined with the off-shell information.

A. Coupling of photons to pions

The electromagnetic form factor of the pion can be parametrized as

$$F_\pi(q^2) = \frac{m_\rho^2}{m_\rho^2 - i m_\rho \Gamma_\rho(q^2) - q^2} \quad , \tag{29}$$

where $m_\rho = 0.77$ GeV is the mass of the ρ meson and

$$\Gamma_\rho(q^2) = 0.2458 \frac{(q^2 - 4m_\pi^2)^{3/2}}{q^2} \Theta(q^2 \geq 4m_\pi^2)$$

describes the decay of the ρ meson into two pions, which is with a contribution of more than 99% the dominant decay channel.

The coupling that leads to such a form factor can be modeled by the following Lagrangian density. Since the only processes of interest for this discussion are those competing with the coupling of a photon to the hadrons, only the neutral vector mesons ρ^0 and ω will be considered

$$\begin{aligned}\mathcal{L} = \frac{1}{2} &\{[\partial_\mu + i(g_{\rho\pi}\rho_\mu + eA_\mu)T_3 + g_{\omega\pi}\omega_\mu]\,\tilde{\pi}\}^\dagger \\ &\times \{[\partial^\mu + i(g_{\rho\pi}\rho^\mu + eA^\mu)T_3 + g_{\omega\pi}\omega^\mu]\,\tilde{\pi}\} \\ &- \frac{1}{2}m_\pi^2 \tilde{\pi}^\dagger \tilde{\pi} - \frac{1}{4}F_{\mu\nu}F^{\mu\nu} + \mathcal{L}_{\rho\gamma} + \mathcal{L}_{\omega\gamma} \ , \end{aligned} \tag{30}$$

$$\mathcal{L}_{\rho\gamma} = -\frac{1}{4}G^\rho_{\mu\nu}G^{\mu\nu}_\rho + \frac{1}{2}m_\rho^2 \rho^\dagger_\mu \rho^\mu - \frac{e}{2g_{\rho\gamma}}F_{\mu\nu}G^{\mu\nu}_\rho \ , \tag{31}$$

$$\mathcal{L}_{\omega\gamma} = -\frac{1}{4}G^\omega_{\mu\nu}G^{\mu\nu}_\omega + \frac{1}{2}m_\omega^2 \omega^\dagger_\mu \omega^\mu - \frac{e}{2g_{\omega\gamma}}F_{\mu\nu}G^{\mu\nu}_\omega \quad , \tag{32}$$

where $G^\rho_{\mu\nu} = \partial_\mu\rho_\nu - \partial_\nu\rho_\mu$, $G^\omega_{\mu\nu} = \partial_\mu\omega_\nu - \partial_\nu\omega_\mu$, $F_{\mu\nu} = \partial_\mu A_\nu - \partial_\nu A_\mu$, $g_{\rho\gamma}$ and $g_{\rho\pi}$ are the coupling constants of the ρ meson to the photon and the pion respectively, and $g_{\omega\gamma}$ and $g_{\omega\pi}$ are those for the ω meson.

Note that with the tensor coupling in the Lagrangian (31) and (32) the photon–vector-meson vertex turns out to be proportional to q^2. In this case the contributions of the vector mesons to the photon polarization function vanish for $q^2 = 0$; the photon thus remains massless very naturally, whereas in the other case more involved constructions are needed to keep the photon mass zero [5]. Also the coupling of the field tensors is gauge invariant by definition.

For the form factor one gets

$$\begin{aligned} F_\pi(q^2) = 1 &+ \frac{g_{\rho\pi}}{g_{\rho\gamma}} \frac{q^2}{m_\rho^2 - i m_\rho \Gamma_\rho(q^2) - q^2} \\ &+ \frac{g_{\omega\pi}}{g_{\omega\gamma}} \frac{q^2}{m_\omega^2 - i m_\omega \Gamma_\omega(q^2) - q^2} \quad . \end{aligned} \tag{33}$$

Complete vector meson dominance (VMD) assumes that $g_{\rho\pi} = g_{\rho\gamma} = g_\rho$ [5] and neglects the coupling to the ω meson completely. Under this assumption (33) reduces to (29). The constants $g_{\rho\pi}$ and $g_{\rho\gamma}$, however, can be inferred from the decay properties of the ρ meson, $\rho \to \pi^+\pi^-$ and $\rho \to \gamma \to e^+e^-$. By converting the measured widths [29] into coupling constants one finds $g_{\rho\pi} = 5.9$ and $g_{\rho\gamma} = 5.1$. So the universality criterion is almost fulfilled, but not exactly.

To calculate the ratio $g_{\omega\pi}/g_{\omega\gamma}$ one uses

$$\frac{g_{\rho\pi}^2/g_{\rho\gamma}^2}{g_{\omega\pi}^2/g_{\omega\gamma}^2} = \frac{\Gamma_{\rho\to\pi\pi} \cdot \Gamma_{\rho\to e^+e^-}}{\Gamma_{\omega\to\pi\pi} \cdot \Gamma_{\omega\to e^+e^-}} = \frac{1}{0.017^2} \quad .$$

This shows that the ω contribution to the form factor is much smaller than that of the ρ. Nevertheless, it shows up in the form factor because of the rather small ω width which results in the structure on top of the wide bump stemming from the ρ meson (see Fig. 5). The picture that emerges is thus a little different from complete VMD: the best agreement with experiment is reached if one relaxes the assumption of vector meson universality and allows all particles, the photon and the vector mesons, to couple

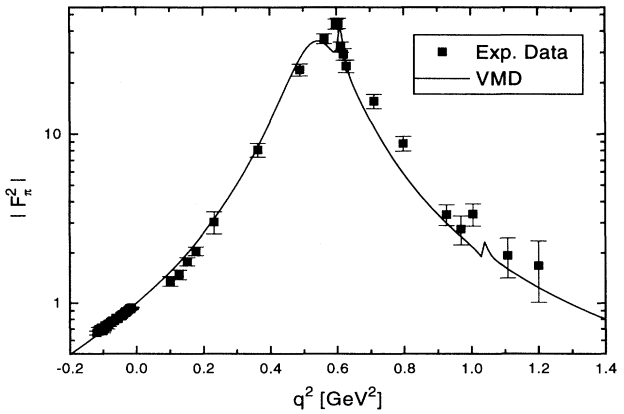

FIG. 5. Electromagnetic form factor of the pion. The data are taken from [23,30,31]; the solid line is obtained using (33) and adding a similar contribution for the Φ meson.

to the hadrons with the appropriate coupling constants. In principle also the phases could be chosen to correctly describe the ρ-ω interference [1]. However, for the arguments in Sec. V the current agreement of data and theory is sufficient.

B. Coupling of photons to baryons

In this subsection the previously developed method will be carried over to baryons, and to the proton in particular. As stated in Sec. II the electromagnetic form factor has an isoscalar and an isovector piece. By the VMD hypothesis these are related to the isoscalar ω meson and to the isovector ρ meson, respectively. If one assumes a Lagrangian density

$$\mathcal{L} = \bar{\Psi}\left[\gamma\cdot\left(i\partial - g_{\rho N}\tau_3\rho^0 - g_{\omega N}\omega - \frac{1}{2}(1+\tau_3)eA\right) - m\right]\Psi + \mathcal{L}_{\rho\gamma} + \mathcal{L}_{\omega\gamma} - \frac{1}{4}F^{\mu\nu}F_{\mu\nu}$$

with $\mathcal{L}_{\rho\gamma}$ and $\mathcal{L}_{\omega\gamma}$ from (31) and (32), one finds

$$F^{s's}_{\substack{i\,\text{proton}\\ \text{neutron}}}(W',W;q^2) = F^{s's}_{i,S}(W',W;q^2) \pm F^{s's}_{i,V}(W',W;q^2) + F^{s's}_{i,\omega}(W',W;q^2)\frac{q^2}{m_\omega^2 - im_\omega\Gamma_\omega(q^2) - q^2} \pm F^{s's}_{i,\rho}(W',W;q^2)\frac{q^2}{m_\rho^2 - im_\rho\Gamma_\rho(q^2) - q^2} \quad . \tag{34}$$

$F^{s's}_{i,S}$ and $F^{s's}_{i,V}$ contain the direct coupling to the photon and $F^{s's}_{i,\omega/\rho}$ contains the coupling to the vector mesons with the appropriate coupling constants. The structure of this Lagrangian density is guided by a gauge principle and thus minimal coupling for the vector meson fields. Additionally there exists a tensor coupling of the form

$$\mathcal{L}^{\text{tensor}} = g_{\rho N}\bar{\Psi}\kappa_\rho\frac{\sigma^{\mu\nu}G^\rho_{\mu\nu}}{4m}\Psi + g_{\omega N}\bar{\Psi}\kappa_\omega\frac{\sigma^{\mu\nu}G^\omega_{\mu\nu}}{4m}\Psi \quad . \tag{35}$$

As a useful example the simplest case with the assumption of no further substructure of the nucleon will now be discussed. It is defined by the Lagrangian given above and neglects all couplings to further mesons like pions. Section V will combine the picture developed in Sec. III with the ideas given below to complete the scenario.

For this simple example one finds $F^{s's}_{i,S}(W',W;q^2) = F^{s's}_{i,V}(W',W;q^2) = 1/2$, $F^{s's}_{i,\omega}(W',W;q^2) = g_{\omega N}/g_{\omega\gamma}$, and $F^{s's}_{i,\rho}(W',W;q^2) = g_{\rho N}/g_{\rho\gamma}$. In principle there will be contributions to F_2 by the tensor coupling of the vector mesons, but these contributions cannot account for the anomalous magnetic moments of proton or neutron since they are weighted with q^2 and thus do not appear for real photons. So the anomalous magnetic moments are genuinely due to the inner structure of the nucleons.

The ratios of the coupling constants can be determined with the help of meson exchange potentials for the nucleon-nucleon interaction; if one takes, e.g., [32] one finds $g_{\rho N}/g_{\omega N} \approx 0.26$. From the ratios of the decay widths one infers $g_{\rho\gamma}/g_{\omega\gamma} = \sqrt{\Gamma_{\omega\to e^+e^-}/\Gamma_{\rho\to e^+e^-}} \approx 0.3$. These ratios are remarkably close to each other, and will in this crude approximation be assumed to be equal. Also from [32] one finds $g_{\rho N}/g_{\rho\pi} \approx 0.47$ which is surprisingly close to 1/2. It must be emphasized, even though this is only a qualitative discussion, that the numbers obtained are close to what is obtained by other authors (Table I). So as a summary one has for the proton

$$F_{1,\text{proton}}(q^2) = 1 + \frac{1}{2}\frac{q^2}{m_\omega^2 - im_\omega\Gamma_\omega(q^2) - q^2} + \frac{1}{2}\frac{q^2}{m_\rho^2 - im_\rho\Gamma_\rho(q^2) - q^2} \quad .$$

For spacelike q^2 and under the further assumption $m_\rho \approx m_\omega \approx m_V$ one finds $F_{1,\text{proton}}(q^2) = m_V^2/(m_V^2 - q^2)$, and $F_{1,\text{neutron}}(q^2) = 0$. This establishes the commonly believed VMD hypothesis. The result falls short of explaining the well established dipole fit to the electromagnetic form factor [1] since it is only of monopole structure.

Concluding, one can state that the pion is essentially structureless, and that probably all of its size, if tested electromagnetically, is due to the ρ meson. The nucleons obviously have structure besides that due to VMD. This is very much in the spirit of Iachello, Jackson, and Lande [16], who introduce a further function to take into account the short-range part of the interaction, or of the two-phase model of Brown, Rho, and Weise [17], who explicitly introduce contributions of the quark core. Also a lot of work has been done to model the structure of the nucleon by taking into account the meson cloud in terms of the exchange of virtual pions [13,14].

TABLE I. Comparison of coupling constants in VMD-like pole fits.

	$g_{\omega N}/g_{\omega\gamma}$	$g_{\rho N}/g_{\rho\gamma}$	
Höhler *et al.* [2]	0.52	0.98	includes πN phase shifts in ρ already
Dubnička [3]	0.376	0.418	remaining strength in higher poles
Gari and Krümpelmann [33]	0.377	0.411	remaining strength in direct coupling

C. Gauge invariance and VMD

At first sight VMD spoils gauge invariance, since even for the free vertex and propagator the WTI is no longer fulfilled in the simple model developed above:

$$q_\mu \Gamma^\mu = e\gamma \cdot q \frac{m_V^2}{m_V^2 - q^2} \neq e\gamma \cdot q \quad .$$

This can be restored by using the same technique as for the pion in Sec. II B. Instead of the γ^μ coupling for the vector mesons a modification can be used:

$$\Gamma^\mu_{VNN} = g_{VN}\left(\gamma^\mu - q^\mu \frac{\gamma \cdot q}{q^2}\right) \quad . \tag{36}$$

This vertex changes only the longitudinal part of the electromagnetic vertex (and thus contributes only to F_3) since $j_\mu \Gamma^\mu_{VNN} = g_{VN} j_\mu \gamma^\mu$ and restores the WTI since now $q_\mu \Gamma^\mu_{VNN} = 0$.

V. RESULTS

Using dispersion techniques, Höhler and Pietarinen [15] pointed out the relation between pion scattering phase shifts and electromagnetic properties of nucleons. Because of a lack of higher lying resonances, it cannot be expected that a simple loop expansion like the one developed here can reproduce the required phase shifts for πN scattering in the entire energy regime under consideration. However, from the Lagrangians (21) and (22) the phase shifts in the $P11$ and $P33$ channels can be successfully calculated close to threshold [34]. On the other hand, the $\pi\pi \to \pi\pi$ amplitude in the $J = T = 1$ channel can be best described by the ρ resonance. All important low energy thresholds are included for $W > m$ by the inelastic channels in the loop expansion, as well as the thresholds for $q^2 > 4m_\pi^2$ by using the correct momentum dependent ρ decay width as shown in Fig. 5. So it is natural, and no double counting is involved, to combine the loop expansion approach (Sec. III) with the idea of vector meson dominance (Sec. IV).

The form factors are thus constructed in three steps. First, all diagrams of Fig. 2 are calculated with the Lagrangians from Sec. III. These diagrams form the contributions to $F^{s's}_{i,S}(W', W; q^2)$ and $F^{s's}_{i,V}(W', W; q^2)$. Next, these diagrams are calculated for a coupling to the neutral vector mesons instead, using the respective experimentally determined coupling constants for the ρ^0 and ω mesons to the hadrons and the photons, resulting in the contributions to $F^{s's}_{i,\rho}(W', W; q^2)$ and $F^{s's}_{i,\omega}(W', W; q^2)$. Combined as in (34), these contributions give the complete irreducible vertex. Solving a system of linear equations (see the Appendix) finally yields the irreducible form factors. The full form factors are obtained by applying (19).

The relevant coupling constants are determined by experiment and symmetry considerations and are given in Table II. The ratios between the couplings of the pion to nucleons and Δ's based on the SU(2)×SU(2) considerations of [35] are carried over to the ρ and ω meson. The absolute values of the ρNN and ωNN vertices are taken from [32]. The $\Delta N\gamma$ coupling constant G_1 is chosen to lie in between the two values from [28].

TABLE II. Coupling constants.

$g_{NN\pi} = 13.45$,	$g_{N\Delta\pi} = 22.86$,	$g_{\Delta\Delta\pi} = 10.76$
$g_{NN\omega} = 8.34$,	$g_{N\Delta\omega} = 14.18$,	$g_{\Delta\Delta\omega} = 6.67$
$g_{NN\rho} = 7.26$,	$g_{N\Delta\rho} = 12.35$,	$g_{\Delta\Delta\rho} = 5.81$
$G_1 = 2.5\ \mathrm{GeV}^{-1}$		
$\kappa_\rho = -6$,	$\kappa_\omega = 0$	
$\Lambda = 1.2$ GeV		

So, besides Λ, no free parameter is involved. Because the cutoff only regularizes the divergent term the results still need to be renormalized. In this paper the following renormalization scheme is employed (quantities with superscript R denote renormalized quantities):

$$W^{*R}(W) = W^*(W) + c_W, \quad m^{*R}(W) = m^*(W) + c_m,$$
$$f_i^{s's\,R} = Z f_i^{s's} \quad .$$

The numbers c_W, c_m, and Z are constants, independent of q^2 or W; they can be determined from Eq. (17). One finds

$$f^{++\,R}_{1,p}(m; q^2 = 0) = \left.\frac{W^{*R} - m^{*R}}{W - m}\right|_{W=m} , \tag{37}$$

where p stands for proton. For the renormalized theory one needs

$$S^{-1}(p) S_0(p) = \Lambda^+(p) \frac{W^{*R} - m^{*R}}{W - m} + \Lambda^-(p) \frac{W^{*R} + m^{*R}}{W + m}$$

$$\xrightarrow[W \to m]{} 1 = \Lambda^+ + \Lambda^- \quad . \tag{38}$$

Comparing the coefficients of the projection operators, it turns out that in this limit $\frac{W^{*R} - m^{*R}}{W - m}$ goes to 1, which is equivalent to the statement that the full propagator has a pole with unit residue at $W = m$. Therefore one has $W^{*R}(m) = m^{*R}(m)$. It cannot be deduced, however, that $W^{*R}(m) = m$ and $m^{*R}(m) = m$, because for $W \to m$ the projector Λ^- becomes zero itself, and thus there is no constraint on $W^{*R}(m) + m^{*R}(m)$.

For a pole of first order one has $\mathrm{Res}[f(z); z_0] = \lim_{z \to z_0}(z - z_0) f(z)$. With the help of this, one can read off from (37) that $1/f^{++\,R}_{1,p}(m; 0)$ is the value of the residue (Res) of the propagator and must thus be equal to 1. This residue is adjusted with the wave function renormalization constant Z. Therefore one must choose $Z = 1/f^{++}_{1,p}(m; 0)$. It turns out that the full form factors are renormalized automatically since, because of Eq. (19), the wave function renormalization constant drops out. In the actual calculation $Z = 0.37$ is found. For the self energies one gets $W^*(m) = m^*(m) = 0.9m$, and thus $\Sigma(m) \approx (0.1\ \mathrm{GeV})(\gamma p - m)$, which is a reasonable value.

A. On-shell form factors

Figure 6 shows the results for the full on-shell form factors $F_{1,2}^{++}(q^2)$ for the proton (a) and (c) and neutron (b) and (d). Note that in this case the full form factor is equal to the irreducible one. The squares are calculated from the dipole fits to $G_E(q^2)$ and $G_M(q^2)$, which describe the data for these momentum transfers up to a few percent in this energy range [1]. In Fig. 6(b), in addition to the dipole fit, information about the deuteron form factor has been taken into account. The two curves of squares correspond to the extreme parametrizations of [36] to indicate the theoretical ambiguities in the description of the NN potential for the deuteron.

A severe test of the model, $F_{1,\mathrm{neutron}}^{++}(q^2 = 0) = 0$, is well fulfilled. For the proton, furthermore, F_1^{++} is reproduced very well. The radius of the proton comes out to be

$$\langle r^2 \rangle = 6 \left. \frac{\partial F_1^{++}(q^2)}{\partial q^2} \right|_{q^2=0} \quad \Rightarrow \quad \langle r^2 \rangle^{1/2} = 0.81 \text{ fm} \quad .$$

F_1^{++} for the neutron is comparable with the data; it falls in between the theoretical uncertainties of the experimental analysis. As discussed in the toy model of Sec. IV, the VMD contribution to the form factor accounts for a monopole shape only. Figure 6 indicates, however, that in the full model a dipole shape is obtained. Therefore it is possible to conclude that, in addition to the explicit treatment of the vector meson pole terms, the π-loop corrections are thus necessary to obtain the experimentally observed dipole shape of the form factors. This conclusion has been discussed previously by Gari and Krümpelmann [33] in a qualitative way, and is in agreement with the findings of early dispersion theory treatment of the form factors. These results give some confidence in the validity of the off-shell results.

Figures 6(c) and 6(d) display the behavior of $F_2^{++}(q^2)$. The shape of the form factor is in agreement with the data in the momentum range plotted; however, it does not show the correct behavior at larger momenta. Furthermore, the model cannot account for the full size of the anomalous magnetic moment. The values found in this calculation are $\kappa_p = 1.45$, $\kappa_n = -1.65$, to be compared with the experimental values of $\kappa_p^{\mathrm{exp}} = 1.79$, $\kappa_n^{\mathrm{exp}} = -1.91$. As mentioned in Sec. IV B, in the Lagrangian given in (31) and (32), there is no contribution of the ρ tensor coupling to F_2 for real photons. This is in contrast to [14], where, by multiplying the bare vertex with $\kappa_\rho/2 \times m_V^2/(m_V^2 - q^2)$, an anomalous magnetic moment is induced. Such a procedure is highly questionable because it can be argued that the tensor coupling of the ρ meson to the nucleon is just due to the loop corrections discussed here [37]. To avoid any double counting the tensor coupling must, therefore, not occur in the direct diagram. In the present calculation, it has been taken into account only for the diagrams with internal radiation to simulate the higher order corrections in a schematic way. This is a crude approximation of the iteration scheme devised in [38]. The tensor coupling influences only the q^2 dependence of F_2, not its magnitude at $q^2 = 0$. A number comparable to the magnetic moment calculated here can be obtained by dividing the result of [14] with a meson cloud by their result for the bare vertex, giving roughly 2/3. Also [13] gets a number which is too small ($\kappa_p \approx 0.5$).

Figure 7 shows the irreducible form factors for projections to negative energy states. f_1^{+-} for the proton is not constrained to 1 by (38). Its value of 0.9 at $q^2 = 0$ is directly related to the scalar and vector self energies. Neither is f_1^{+-} for the neutron constrained to 0. The magnetic form factors show a change of sign as one goes to higher q^2. Their values at $q^2 = 0$ are drastically different from $f_2^{++}(q^2 = 0)$. The full form factors F_i^{+-} can be obtained by rescaling f_i^{+-} by 1/0.9. Even though these form factors never play a role in experiments, they already indicate that all theoretical calculations that rely on the asumption F_i^{++}=F_i^{+-} are incorrect.

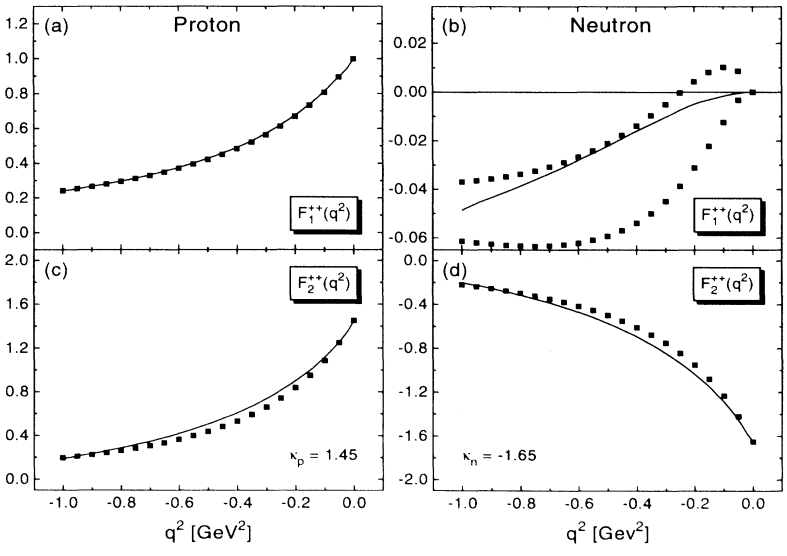

FIG. 6. $F_{1,2}^{++}(m, m; q^2)$ for (a) and (c) proton and (b) and (d) neutron. The solid line is the model calculation; the symbols represent experimental results as explained in the text. For F_2 the experiment is rescaled to the anomalous magnetic moment of this calculation.

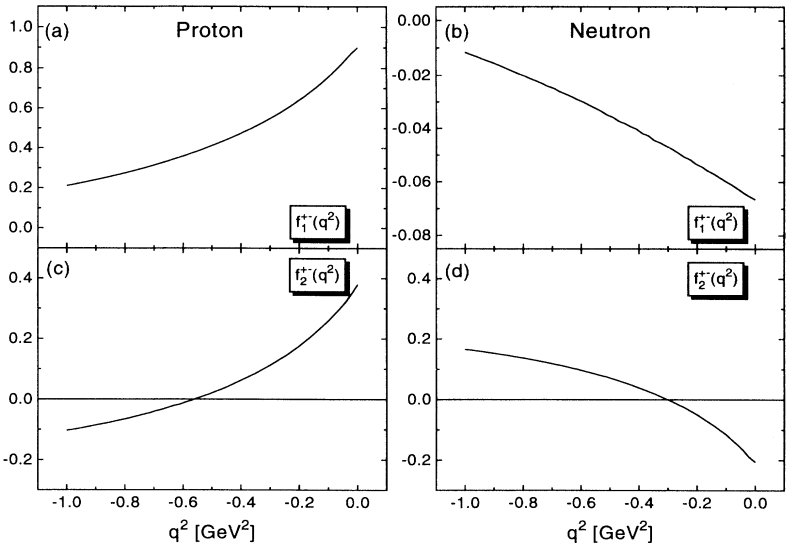

FIG. 7. $f_{1,2}^{+-}(m,m;q^2)$ for (a) and (c) proton and (b) and (d) neutron.

The models [13,14,25] all approximately agree with each other for the electric form factor. Since their magnetic moments are off by more than 50% from experiment, an important process must have been missed in all these calculations. There exists strong experimental evidence that a large part of the magnetic moment is due to spin flip transitions, especially to the Δ resonance [18]. The present calculation shows that about half of the magnetic moment is carried by the diagram with the $\Delta \to N\gamma$ decay mode, which is dominantly $M1$, a mode that was not included in [13,14,25].

It must be stressed that the underestimation of κ does *not* depend on the cutoff Λ used in the calculation. Figure 8 displays the Λ dependence of κ_p and κ_n. The magnetic moments are optimal in the 1 GeV region, giving confidence in the combination of the regularization and renormalization scheme employed. One clearly finds for the larger values of Λ that the magnetic moment decreases. Also for small Λ there is the onset of a decrease, which shows that the choice of the cutoff parameters cannot solve the disagreement. This is in strong contrast to [37], where the tensor coupling increases monotonically with Λ. The difference can be traced to the renormalization procedure of [37], where a subtractive renormalization is used, which is valid only if the wave function renormalization constant is close to 1; this certainly is not the case in the present calculation ($Z = 0.37$). Note that the agreement of state of the art soliton models that include the Δ resonance [12] with the magnetic moment is of the same quality as the agreement of the model presented here.

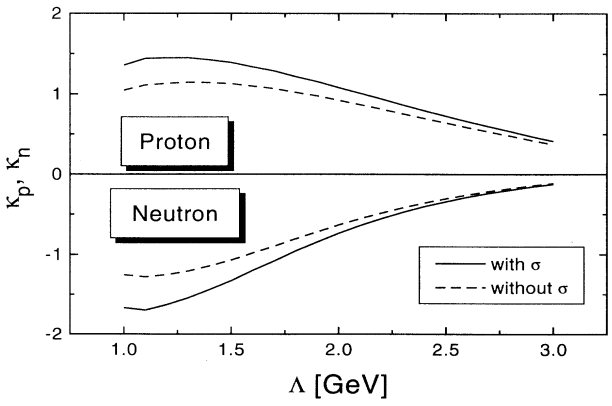

FIG. 8. The anomalous magnetic moment for proton and neutron as function of the cutoff parameter Λ. The solid and dashed lines display the result with and without contributions of the σ meson, respectively.

Bos *et al.* [25] dress the nucleon with a scalar/isoscalar cloud. They use a σ meson with a mass of $m_\sigma = 0.8$ GeV. Since in this case the photon only couples to the nucleon, this gives a large weight to the core contributions. Still, the magnetic moment is only around 0.7. If a contribution like this is included in the present calculation, there is some effect, which is displayed by the dashed line in Fig. 8. The parameters chosen here are $m_\sigma = 0.56$ GeV, $g_\sigma = 11$. The effect is due to a reduction of the wave function renormalization Z. This increases the magnetic moments somewhat; however, without coming anywhere close to the experimental point.

B. Spacelike half-off-shell form factors

Figures 9 and 10 show the off-shell dependence of $F_1^{+\pm}(W;q^2)$ and $F_2^{+\pm}(W;q^2)$ for the proton. In order to see the effects of the pure loop corrections all contributions due to VMD were switched off in the upper panels. Part of the purpose of the following discussion is to show that not only in the timelike electromagnetic form factor can one see the influence of the $N\bar{N} \to \pi\pi$ scattering [15], but also in the half off-shell form factors.

The left column of Fig. 9 shows F_1^{++}. For $W < 1.2$ GeV the slope of the real part of F_1^{++} increases with W, corresponding to an increasing charge radius, which is in agreement with [13,14]. The figure shows that for W above 1.4 GeV the radius stays more or less constant; the

real part falls rather linearly with $-q^2$. The imaginary part reflects the possibility that the incoming nucleon is far enough off shell to decay into final states of one or two pions plus a nucleon or a Δ during the electromagnetic scattering process. Because of the various inelastic thresholds, the imaginary part is expected to depend on the phase space of the decay products. This phase space dependence, however, is mixed with self energy corrections due to the WTI, which themselves have imaginary parts. Thus the imaginary part of F_1^{++} does not show a clear behavior as q^2 and W increase. The absolute value of the form factor including VMD shows only slight dependence on the off-shellness of the incoming proton for F_1^{++}.

For F_1^{+-} (right column of Fig. 9) the situation is different; above $W = 1.4$ GeV it rises fast. Even after including VMD, the changes due to off-shellness are clearly visible. Calculations of cross sections for electromagnetic processes including off-shell nucleons and the correct form factors must be performed in order to show the importance of the negative energy components.

For the magnetic form factor $F_2^{+\pm}$ (Fig. 10) there is a dramatic change in shape for the larger values of W in the real part, whereas the imaginary part mainly seems to grow with phase space. At $q^2 = 0$ the real part of $F_2^{+\pm}$ develops a maximum as a function of W between $W^2 = 1.4$ GeV^2 and $W^2 = 2$ GeV^2; the absolute value, on the other hand, increases rather smoothly.

A detailed analysis of the contributions of specific diagrams to the full form factor reveals that the above effects are caused by the meson cloud. Figure 11 shows the decomposition for $W = 0.939$ GeV and $W = 1.4$ GeV in comparison. The full symbols show contributions of radiating pions [Figs. 2(c)–2(e)], i.e., the meson cloud; the open symbols correspond to radiating baryons [Fig. 2(b)], i.e., the core. Squares describe diagrams with an internal nucleon and circles represent diagrams with a propagating Δ. The solid line is the contribution of the direct diagram [Fig. 2(a)] and is counted as a core contribution. Contributions from the diagram of Fig. 2(f) are indicated by dashed lines.

It is quite important to notice that for F_1 for both

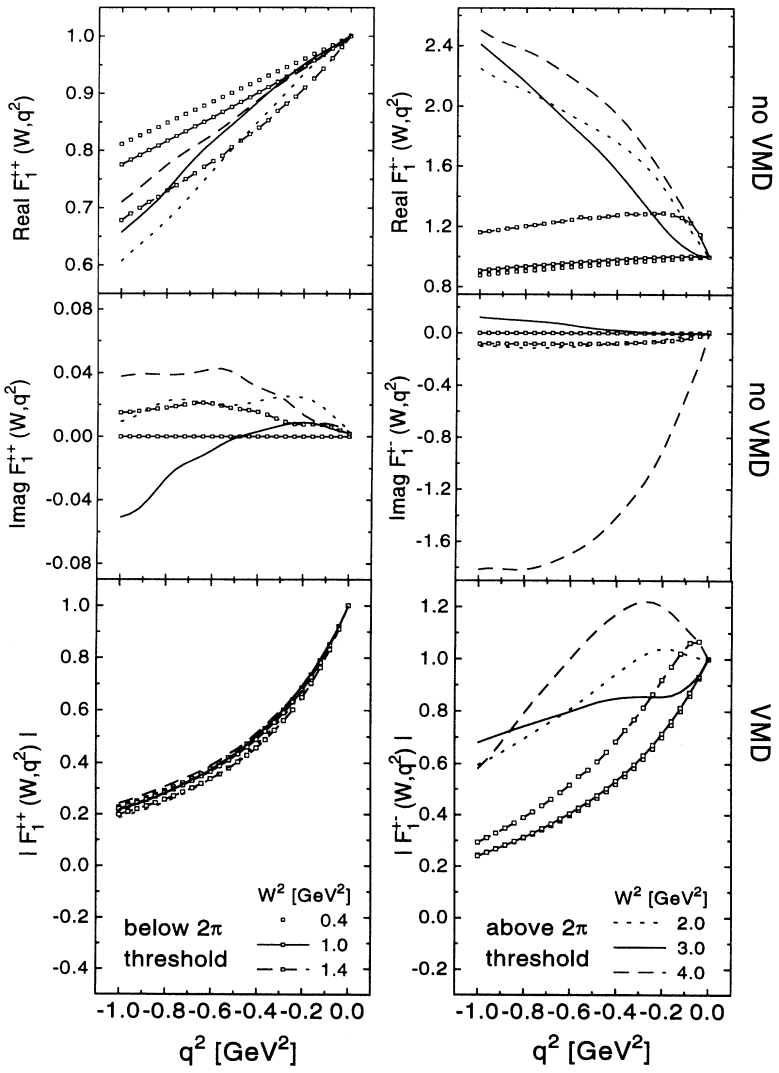

FIG. 9. Half off-shell form factors of the proton in the spacelike region. The left panel displays $F_1^{++}(W;q^2)$ for several incident invariant masses. The curves with symbols are below the 2π threshold; the curves without symbols are above. The two upper plots show real and imaginary parts of the form factor without VMD contributions, while the lower plot shows the absolute value including VMD. The right panel displays $F_1^{-+}(W;q^2)$ in the same way.

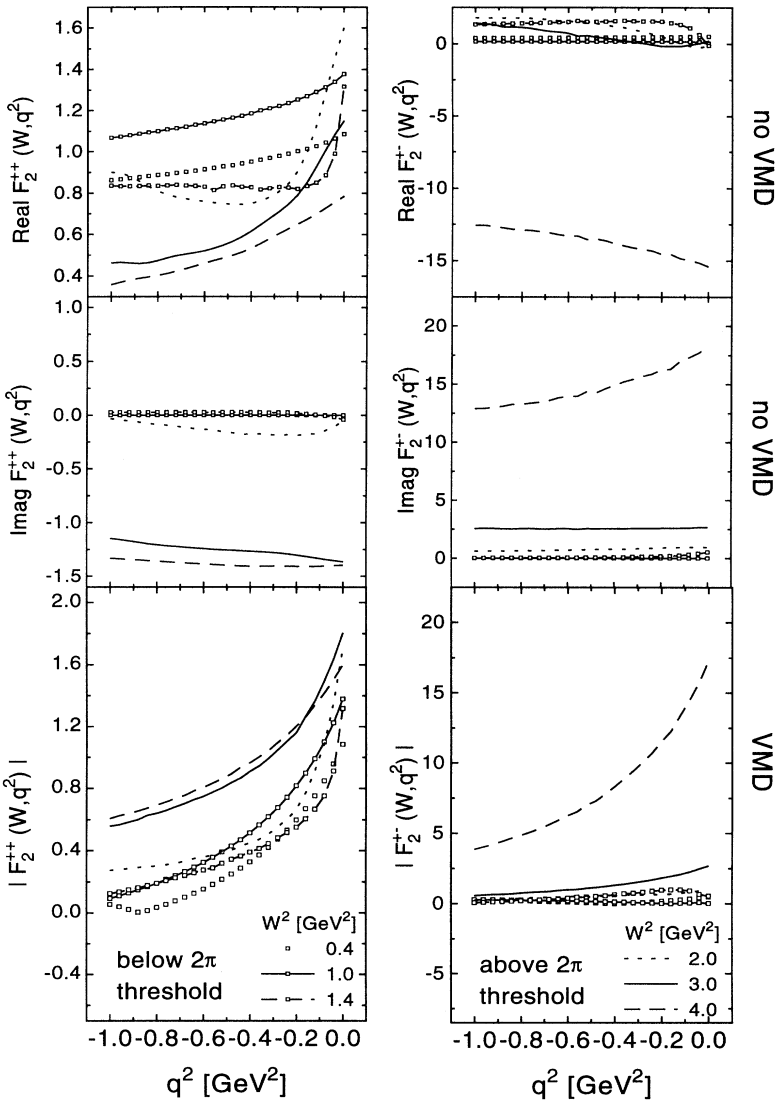

FIG. 10. Same as Fig. 9 but for $F_2^{\pm+}(W;q^2)$.

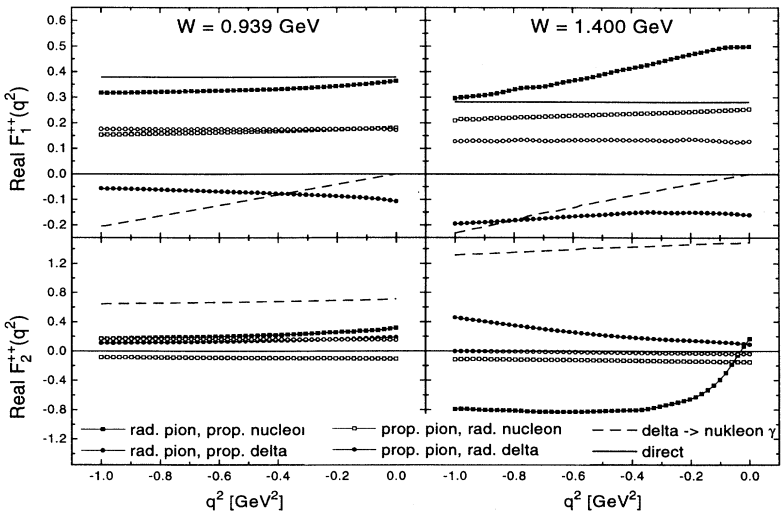

FIG. 11. Detailed analysis of the contribution of the single diagrams in the $W = 1.4$ GeV case (right panel) compared to the on-shell case (left panel) for the proton. Lines with full symbols correspond to meson cloud contributions, lines with open symbols and the full line are core contributions. The dashed line represents the $\Delta \rightarrow N\gamma$ decay contribution.

values of W the cloud contributions appear with different sign, leaving a more dominant core, whereas for F_2 the core contributions, at least for $W = m$, tend to cancel. So while F_1 is core dominated, F_2 is more influenced by the meson cloud. The most important contribution to F_2 is the transition of the Δ, in agreement with the analysis of the Gerasimov-Drell-Hearn sum rule [18].

An obvious change in F_1^{++}, if one goes off shell, is the increased importance of the meson cloud from 15% to 35%. This is clearly an important sign that the mesonic excitations must be carefully treated in all models for off-shell form factors. Already in the on-shell case the contributions with a propagating Δ are of some importance.

From the slopes one can deduce that the contributions of radiating pions (cloud) reach further out than those of radiating baryons (core). Since the different contributions show different slopes at $q^2 = 0$, which is especially true for the off-shell case, it is not possible to give an adequate parametrization of the q^2 dependence of the form factor using a single parameter, if one wants to maintain a cloud/core picture to describe the extension of the nucleon, as in the semiphenomenological models of [16,17]. This is even more clearly visible for the magnetic form factor.

In going from the on-shell point to 1.4 GeV, the major changes come from the diagrams 2(c)–2(e), which all contribute to the cloud. For F_1^{++} these fall off faster at 1.4 GeV; for F_2^{++} the shape is completely determined by these diagrams and all other contributions stay rather constant. A further analysis of the cloud contribution shows that the diagrams containing the contact term do not show drastic changes in shape. So the responsible diagram is 2(c). This diagram is the only one that allows for the 2π decay. Since this decay mode is not incorporated in the self energy diagrams at the present level of the loop expansion, its threshold behavior cannot be changed by the WTI. This leads to the assumption that this effect is caused by the 2π threshold. Including a more realistic treatment of the Δ decay width is not expected to change this picture, because once again the WTI will diminish the threshold effects.

C. Timelike form factors

Figures 12 and 13 show the electric and magnetic form factors for the proton, respectively, in the entire range covered by this calculation. The contour lines show $\log_{10}|F_{1,2}^{++}(W^2;q^2)|$. Various thresholds are indicated by dotted lines. The region which is not accessible by experiments (unphysical region) is indicated by the white area; all dispersion relation approaches rely on analytical continuation into this region.

It must be emphasized that at this level all inelasticities up to the 2π channel are included in the vertex either by the $\rho \to \pi\pi$ decay, or by $N^* \to X + n\pi$ $(n = 1, 2)$. While F_1 shows almost no changes as one goes off shell, for F_2 the influence of inelastic channels remains visible. The behavior of the meson cloud contributions influences the form factor. A change of F_2 at the various thresholds can be observed. Since at the 2π threshold the contributions are suppressed because the pions are in a relative p-wave state, the influence of this channel increases smoothly with momentum, as can be seen in Fig. 13.

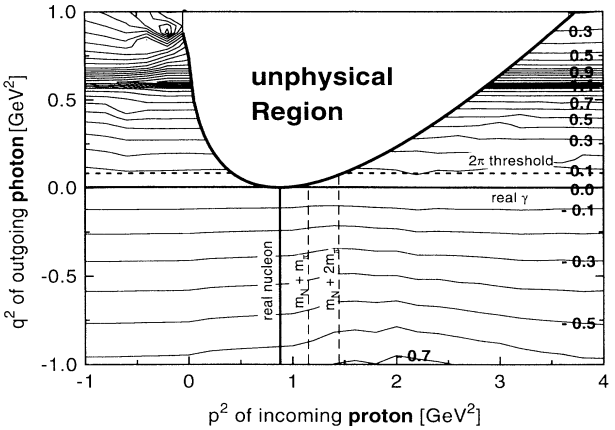

FIG. 12. F_1^{++} for the proton in the full range of applicability of the model. The contour lines are steps of 0.1 in $\log_{10}|F|$. Various thresholds are indicated by dashed lines. The white region is experimentally inaccessible.

It is due to the WTI that F_1 does not change very much when going off shell. Each off-shell effect in the vertex is nearly canceled by the self energy corrections (19), which have the same thresholds. Interestingly, this cancellation seems to be independent of q^2. This is not entirely true (see the last subsection); however, the q^2 dependence is so much dominated by VMD that other effects, which depend on q^2, are hardly visible. This is a very important result. If VMD exists for nucleons as well as for pions, it will clearly be observable, since it is not reduced for off-shell nucleons in the case of F_1, and is still dominant for F_2.

For $W = 2$ GeV Fig. 14 displays the scalar and vector contributions of the direct coupling graphs and of vector meson graphs to the form factors. From this information the proton or neutron form factor can be constructed. For $F_{1S/V}$ it shows a smooth behavior; the minimum in the vector imaginary part is due to the $\pi^+\pi^-$ channel.

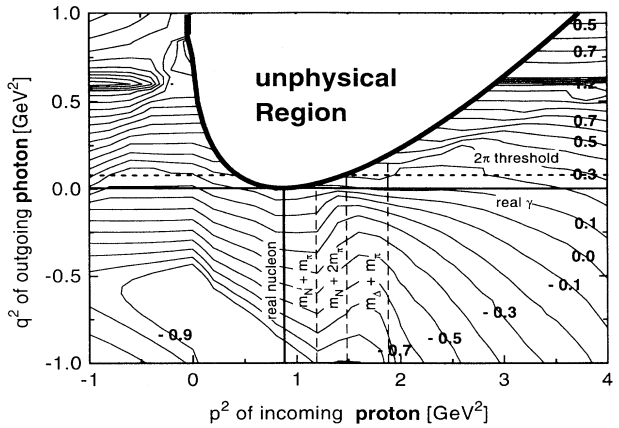

FIG. 13. Same as Fig. 12, but for F_2^{++}.

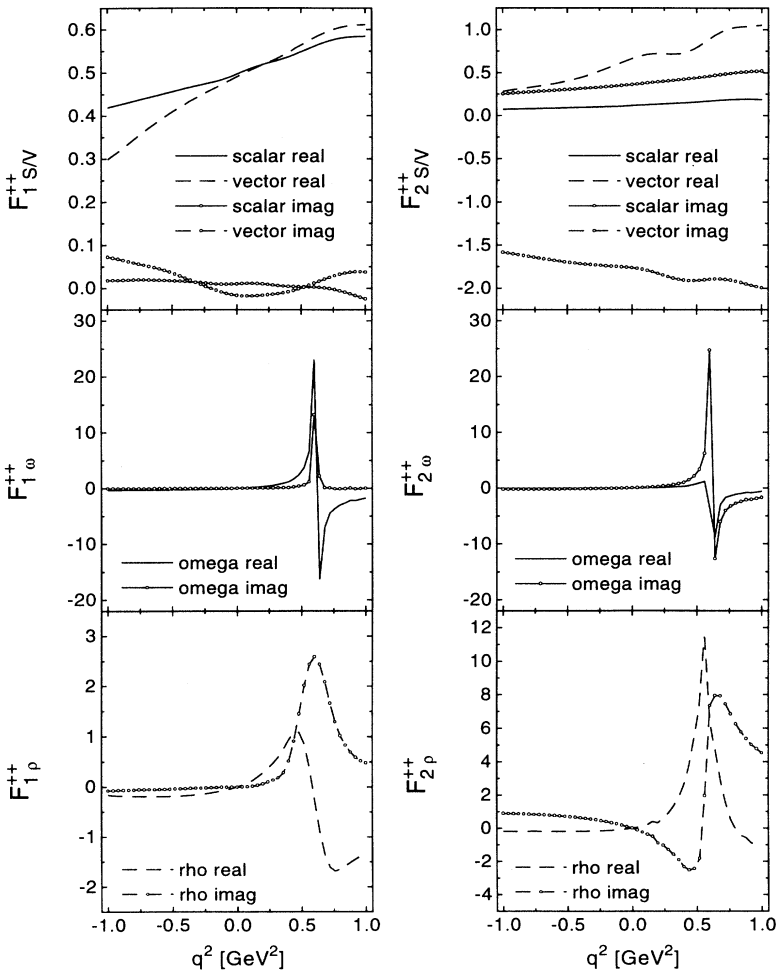

FIG. 14. Real and imaginary parts of scalar and vector contributions to the electric form factor for $W = 2$ GeV. The full lines display the isoscalar contributions; the dashed lines display the isovector ones. Symbols indicate imaginary parts. The upper plots show the scalar and vector contributions of the direct photon coupling. The plots below show contributions of ω and ρ mesons separately.

The pure photon channels are clearly least important as compared to the vector meson channels. The figure shows the broad ρ and the narrow ω resonance. Since both mesons couple to the nucleon with about equal strength, the ω contribution is an order of magnitude larger than the ρ contribution at peak level because of the ω's small width. Note that in the case of F_2 for the vector meson contributions the role of the imaginary and real parts has changed, indicating that the imaginary part of the loop expansion without VMD is significantly larger than its real part. This is consistent with the situation in the spacelike sector (Fig. 10) and gives rise to interference. For F_2 the contribution of the ρ meson is of larger importance than for F_1.

To show once again that VMD can be observed even in an experiment involving a half off-shell vertex, a cut of Fig. 12 is plotted in Fig. 15. The absolute magnitudes of the single contributions in the photon, ω, and ρ channels as well as the absolute magnitude of the coherent sum are displayed for timelike momentum transfers for the proton and the neutron at $W = 2$ GeV. Despite the small width of the ω resonance it is not possible to resolve the ρ contribution in F_1. The sum is almost exclusively exhausted by the ω contribution, while the ρ on the other hand is only visible as a broad background. On the other hand, for F_2 the ρ component is not much smaller than the ω component; therefore subtle interference effects show up between the ρ and ω channels, which might be accessible in experiments on both protons and neutrons.

Experiments on dilepton production in $p+A$ reactions, where the $\pi^+\pi^-$ annihilation channel is suppressed, may thus offer a chance to study medium modifications of the

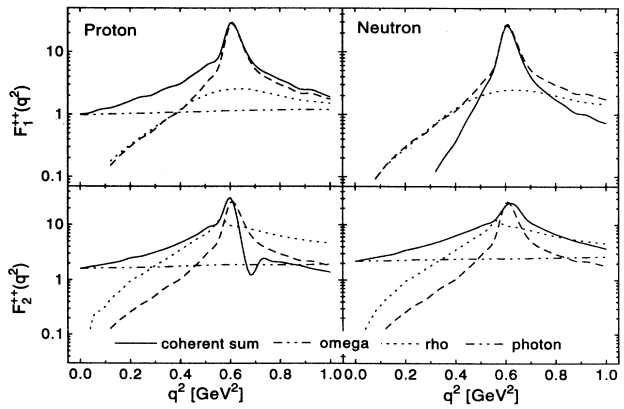

FIG. 15. Decomposition of $|F_{1,2}^{++}|$ for the proton (left) and neutron (right) at $W = 2$ GeV into components coming from the direct photon vertex, the ρ meson vertex, and the ω meson vertex. The sum is the result of a coherent superposition of the single contributions.

ω meson from the electromagnetic properties of the nucleon in the same way as medium modifications of the ρ meson from electromagnetic properties of the pion. Because the nucleon's form factors are larger than that of the pion (at peak position $|F_\pi| \approx 7$), they are visible even in heavy ion collisions above the background from $\pi^+\pi^-$ annihilation [9]; however, a very good resolution of the experimental apparatus is required to resolve them.

VI. SUMMARY

To study the production of dileptons in high energy nuclear reactions one needs information about the half off-shell timelike electromagnetic form factors, which are unknown until now. We have, therefore, constructed a dynamical model based on a hadronic framework to calculate the electromagnetic form factors for momentum transfers of the photon of $-1\ \mathrm{GeV}^2 < q^2 < 1\ \mathrm{GeV}^2$ and for nucleons with $-1\ \mathrm{GeV}^2 < p^2 < 4\ \mathrm{GeV}^2$.

Starting from an expansion of the nucleon propagator in pion loops, the electromagnetic vertex is constructed by inserting external photons to each charged particle line, thus obeying the constraints due to the WTI. Together with the concept of VMD, this approach includes at least schematically all findings of the spectral analysis of the late 1960s [15]. It is possible to maintain the cloud/core picture that proved successful in semiphenomenological models [16,17]. It is important to include the Δ resonance to reproduce the magnetic properties, which is in accord with an analysis of the Gerasimov-Drell-Hearn sum rule [18]. The coupling constants and the cutoff are chosen in agreement with meson exchange models and symmetry considerations [35].

The momentum dependence of the spacelike on-shell form factors is reproduced. The charge radius of the proton is found to be $r = 0.81$ fm. The electric form factor of the neutron falls in between the uncertainties of the data analysis. The magnetic moments are $\kappa_p = 1.45$ and $\kappa_n = -1.65$, which are much closer to the experimental values than in comparable calculations [13,14], but still too small. The better agreement can be traced to the $\Delta \to N\gamma$ decay process, which occurs in neither of the above cited works. A decomposition of the form factors shows that for F_1 the core contributions dominate, while for F_2 the cloud is more important. It also shows that inelastic thresholds influence the form factors. However, for F_1 the dependence is only weak because it is compensated by self energy corrections required by gauge invariance. For F_2 threshold effects remain visible. The change of the contributions of the meson cloud is larger than that of the core contributions.

The weak off-shell effects enable one to study VMD in the experimentally accessible region of the (W, q^2) plane. It turns out that only the signal of the ω meson can clearly be extracted; the ρ meson contributions only result in a broad background. As an effect one has the possibility to study medium effects on the ω very clearly by measuring the electromagnetic form factor in $p + A$ and even in heavy ion collisions.

It is found that calculations which are based on the assumption that $F_i^{++} = F_i^{+-}$ must be rechecked.

The model for the vertex used here certainly leaves room for improvements. Taking into account higher resonances, especially of spin 3/2, as well as heavier mesons will help to improve the magnetic moments. The finite decay width of the Δ also needs to be incorporated. Since it has an effect on the self energy as well as on the vertex, it is expected that due to the WTI the off-shell behavior of the form factors will not change appreciably.

ACKNOWLEDGMENTS

Interesting discussions with members of the DLS group and with György Wolf are greatly appreciated. A hint of T. Maruyama concerning numerical integration was extremely helpful. This work was supported by BMFT and GSI Darmstadt.

APPENDIX: NUMERICAL DETAILS

The sum of all Feynman diagrams in Fig. 2 results in the irreducible vertex. To obtain the form factors from the most general vertex (4) the projection on positive/negative energy must be performed for in- and outgoing nucleons:

$$\Lambda^{s'}(p')\Gamma^\mu(p',p)\Lambda^s(p) = \Lambda^{s'}(p')\sum_{i=1}^{3} f_i^{s's}(W',W;q^2)\mathcal{O}_i^\mu\Lambda^s(p) \quad . \tag{A1}$$

Performing traces over contractions of the vertex with three linear independent four-vectors $v_1^\mu = P^\mu = p'^\mu + p^\mu$, $v_2^\mu = q^\mu = p'^\mu - p^\mu$, $v_3^\mu = \gamma^\mu$ gives

$$\tilde{T}_i = \mathrm{Tr}\ v_i^\mu\Lambda^{s'}(p')\Gamma_\mu\Lambda^s(p) = \sum_{j=1}^{3} a_{ij} f_j^{s's} \quad . \tag{A2}$$

The same procedure is performed with the sum S_μ of all contributing Feynman diagrams:

$$T_i = \mathrm{Tr}\ v_i^\mu\Lambda^{s'}(p')S_\mu\Lambda^s(p) \quad . \tag{A3}$$

To obtain the form factors one must equate (A2) and (A3):

$$T_i = \tilde{T}_i = \sum_{j=1}^{3} a_{ij} f_j^{s's} \quad . \tag{A4}$$

While the expressions $\tilde{T}_i$ can be obtained analytically, the quantities T_i must be calculated numerically. They can be decomposed into integrals of the following form:

$$T_i = \sum_d \sum_{u,v,w} c^{ds's}_{u,v,w}(p'^2, p^2, q^2) \times \int \frac{d^4k}{(2\pi)^4} \left[(p'k)^u (pk)^v (k^2)^w / N_d(p', p, k)\right] \quad .$$

The index d labels the different diagrams contributing to S_μ. $N_d(p', p, k)$ contains the denominator of the propagators in diagram 2(d).

The coefficients $c^{ds's}_{u,v,w}(p'^2, p^2, q^2)$ as well as the a_{ij} in Eq. (A2) are calculated using the high energy package of REDUCE [39].

All integrals are of the form

$$I(p', p) = \int \frac{d^4k}{(2\pi)^4} \frac{(p'k)^u (pk)^v (k^2)^w}{\prod_{p=1}^{N} \left[(a_p - k)^2 - m_p^2 + i\epsilon\right]} \quad ,$$

where a_p and m_p are the specific momenta and masses of the propagators in the diagrams. The number N of factors in the denominator depends on the choice of monopole or dipole cutoff and ranges from 4 to 7. The integrals are performed numerically.

$I(p', p)$ is solved in the rest frame of the outgoing nucleon, which always exists in the case of half off-shell kinematics. The integration of k^0 is done by contour integration around the poles of $\prod_{p=1}^{N}[(a_p - k)^2 - m_p^2 + i\epsilon]^{-1}$. Let k_i^0 denote the poles in the upper half plane. Since not all poles are of first order, for each $\vec{k}$ the residue must be calculated by taking numerical derivatives:

$$I(p', p) = i \int \frac{d^3k}{(2\pi)^3} \sum_{i=1}^{n} \mathrm{Res}(k_i^0) \quad , \tag{A5}$$

$$\mathrm{Res}(k_i^0) = \frac{1}{(n_i - 1)!} \frac{d^{n_i - 1}}{dk^{0\,n_i - 1}} \times \left[\frac{(p'k)^u (pk)^v (k^2)^w (k^0 - k_i^0)^{n_i}}{\prod_{p=1}^{N} \left[(a_p - k)^2 - m_p^2 + i\epsilon\right]} \right]_{k^0 = k_i^0} ,$$

where n_i is the order of the pole at k_i^0. For spacelike momentum transfer the sum of the residues is a well behaved function of $\vec{k}$. However, in the timelike region it still has poles because of the physical inelasticities for $q^2 \geq 4m_\pi^2$ and $p^2 \geq (m + m_\pi)^2$. These poles are treated with a subtraction technique, which will be described below. Since the momenta p' and p can be chosen such that I is invariant under rotations about the z axis, the ϕ integration is trivial. The remaining integration is two dimensional. From now on k denotes $|\vec{k}|$

$$I(p', p) = \int_{-1}^{1} dx \int_0^\infty dk \frac{f(k, x)}{g(k, x)} \qquad \text{with} \qquad x = \cos\theta \ .$$

Let $k_i(x)$ be defined by $g(k_i(x), x) = 0$ $(i = 1, 2)$. The $k_i(x)$ are complex functions of x. For $x \geq x_0$ the imaginary part becomes $\pm\epsilon$. Below x_0 an ordinary integration can be used. Above x_0 the integral $I(p', p)$ splits into a principal value integral and an imaginary part

$$\begin{aligned} \int_0^\infty dk \frac{f(k,x)}{g(k,x)} &= \int_0^\infty dk \frac{f(k,x)}{g_R(k,x)} \frac{1}{\prod_{i=1}^{2} [k_i(x, \epsilon = 0) - k + i\epsilon \mathrm{Re}(dk_i/d\epsilon)]} \\ &= P \int_0^\infty dk \frac{f(k,x)}{g_R(k,x)} \frac{1}{[k_1(x,\epsilon=0) - k][k_2(x,\epsilon=0) - k]} \\ &\quad - i\pi \frac{f(k_1(x), x)}{g_R(k_1(x), x)} \frac{\mathrm{sgn} dk_1/d\epsilon}{k_2(x) - k_1(x)} \Theta(k_1(x)) \\ &\quad - i\pi \frac{f(k_2(x), x)}{g_R(k_2(x), x)} \frac{\mathrm{sgn} dk_2/d\epsilon}{k_1(x) - k_2(x)} \Theta(k_2(x)) \ . \end{aligned} \tag{A6}$$

Since $P\int_0^\infty 1/(k^2 - k_0^2)dk = 0$, the principal value integral is treated as follows:

$$P \int_0^\infty dk \frac{f(k,x)}{g(k,x)} = \int_0^\infty dk \left[\frac{f(k,x)}{g(k,x)} - \sum_{i=1}^{2} \frac{f(k_i(x), x)}{k^2 - k_i^2(x)} \frac{k^2 - k_i^2(x)}{g(k,x)} \bigg|_{k = k_i(x)} \Theta(k_i(x)) \right] \quad .$$

The integrand is now finite for all k.

If $p^2 \geq (m + 2m_\pi)^2$, then in some diagrams both functions $k_i(x)$ contribute to the imaginary part. In this case there is a remaining singularity of the type $1/\sqrt{1 - (x/x_0)^2}$ at $x = x_0$. The integral is thus converging, but numerically unstable. It can be treated by a trick similar to the one used above:

$$\int_{-|x_0|}^{|x_0|} \frac{\varphi(x)}{\sqrt{x_0^2 - x^2}} dx = \int_{-|x_0|}^{|x_0|} \frac{\varphi(x) - \varphi(x_0)}{\sqrt{x_0^2 - x^2}} dx + \pi\varphi(x_0) \ .$$

After having calculated all integrals in T_i, Eqs. (A4) are solved for the invariant form factors.

Numerical inaccuracies can occur at various points. For example, in (A5) only the sum of all residues falls off fast enough in k so that the integral converges. There is a delicate cancellation of the summands, which can be shown analytically, that is hard to reproduce by taking numerical derivatives. Furthermore, for large k the poles come near to each other, sometimes too close to take the numerical derivative with good enough accuracy. This is worked around by not evaluating the integrand at too

large values of k. A cutoff is chosen dynamically if the integrand is small enough. For higher values of k asymptotic behavior is assumed and the integral is solved analytically. Unfortunately, under this assumption the WTI suffer. They are only fulfilled at the 1% level.

In (A6) problems arise when $|x_0|$ is close to 1. Then too few grid points of the integration mesh contribute to the imaginary part. In these cases additional grid points are created and integration weights are redistributed such that the integral is performed over at least 10 grid points in the $\cos\theta$ direction.

The numerical difficulties are best under control for a very simple integration with equally spaced grid points of equal weights. To obtain an acceptable accuracy up to 400 points in the radial direction and 100 points in the $\cos\theta$ direction are used.

[1] M. Gourdin, Phys. Rep. **11**, 29 (1974).
[2] G. Höhler *et al.*, Nucl. Phys **B114**, 505 (1976).
[3] S. Dubnička, Nuovo Cimento A **103**, 1417 (1990).
[4] G. Bardin *et al.*, Phys. Lett. B **257**, 514 (1991).
[5] J. J. Sakurai, *Currents and Mesons* (University of Chicago Press, Chicago, 1969).
[6] M. Schäfer *et al.*, Nucl. Phys. **A572**, 429 (1994).
[7] G. Roche *et al.*, Phys. Rev. Lett. **61**, 1069 (1988).
[8] Gy. Wolf *et al.*, Nucl. Phys. **A517**, 615 (1990).
[9] Gy. Wolf, GSI Report No. 94-1, 1994.
[10] T. Feuster *et al.*, in Proceedings of the XXXII International Winter Meeting on Nuclear Physics, Bormio, 1994, edited by I. Iori.
[11] M. Schäfer, H. C. Dönges, and U. Mosel, Report No. UGI-94-6, 1994.
[12] A. Z. Górski, Chr. V. Christov, and K. Goeke, Report No. RUB-TP II-56/93, 1993.
[13] H. W. L. Naus and J. H. Koch, Phys. Rev. C **36**, 2459 (1987).
[14] P. C. Tiemeijer and J. A. Tjon, Phys. Rev. C **42**, 599 (1990).
[15] G. Höhler and E. Pietarinen, Phys. Lett. **53B**, 471 (1975).
[16] F. Iachello, A. D. Jackson, and A. Lande, Phys. Lett. **43B**, 191 (1973).
[17] G. E. Brown, M. Rho, and W. Weise, Nucl. Phys. **A454**, 669 (1986).
[18] V. Burkert and Z. Li, Phys. Rev. D **47**, 46 (1993).
[19] A. M. Bincer, Phys. Rev. **118**, 855 (1960).
[20] J. D. Bjorken and S. D. Drell, *Relativistic Quantum Mechanics* (McGraw-Hill, New York, 1964).
[21] J. C. Ward, Phys. Rev. **78**, 182 (1950); Y. Takahashi, Nuovo Cimento **6**, 370 (1957).
[22] F. Gross and D. O. Riska, Phys. Rev. C **36**, 1928 (1987).
[23] A. Quenzer *et al.*, Phys. Lett. **76B**, 512 (1978).
[24] T. Ericson and W. Weise, *Pions and Nuclei* (Clarendon Press, Oxford, 1988).
[25] J. W. Bos, S. Scherer, and J. H. Koch, Nucl. Phys. **A547**, 488 (1992).
[26] W. Rarita and J. Schwinger, Phys. Rev. **60**, 61 (1941).
[27] G. E. Brown and W. Weise, Phys. Rep. **22**, 279 (1975).
[28] H. F. Jones and M. D. Scadron, Ann. Phys. (N.Y.) **81**, 1 (1973).
[29] Particle Data Group, Phys. Rev. D **45**, S1 (1992).
[30] S. R. Amendolia *et al.*, Phys. Lett. **146B**, 116 (1984).
[31] S. R. Amendolia *et al.*, Phys. Lett. **138B**, 454 (1984).
[32] F. Gross, J. W. Van Orden, and K. Holinde, Phys. Rev. C **45**, 2094 (1992).
[33] M. Gari and W. Krümpelmann, Z. Phys. A **322**, 689 (1985).
[34] E. Oset, H. Toki, and W. Weise, Phys. Rep. **83**, 281 (1982).
[35] G. E. Brown *et al.*, Phys. Lett. **118B**, 39 (1982).
[36] S. Platchkov *et al.*, Nucl. Phys. **A510**, 740 (1990).
[37] J. Flender and M. F. Gari, Z. Phys. A **343**, 467 (1992).
[38] D. Plümper, J. Flender, and M. F. Gari, Phys. Rev. C **49**, 2370 (1994).
[39] REDUCE *User's Manual*, The Rand Corporation, Santa Monica, 1984.